https://doi.org/10.5194/egusphere-2026-5468
Preprint. Discussion started: 11 September 2026
© Author(s) 2026. CC BY 4.0 License.

A disruption scoring framework for critical infrastructure exposed to multiple hazard sources: tephra fall on Japan's electricity network

Rui Xue Natalie Teng[1], Josh L. Hayes[2], Susanna F. Jenkins[1], David Lallemant[1], Mathis Joffrain[3], Eisuke Fujita[4], John Wardman[5], Yousuke Miyagi[4], Tomohiro Kubo[6]

[1]Earth Observatory of Singapore, Asian School of the Environment, Nanyang Technological University, Singapore, 639798, Singapore
[2]Earth Sciences New Zealand, Lower Hutt, 5040, New Zealand
[3]AXA, Paris, 75008, France
[4]National Research Institute for Earth Science and Disaster Resilience, Tsukuba, 305-0006, Japan
[5]Maximum Information, London, EC4R 0AN, United Kingdom
[6]Mount Fuji Research Institute, Fujiyoshida, 403-0005, Japan

Correspondence to: Rui Xue Natalie Teng (natalie.tengrx@ntu.edu.sg) and Susanna F. Jenkins (susanna.jenkins@ntu.edu.sg)

Abstract. Assessing how hazards disrupt critical infrastructure systems is challenging, as these systems often comprise spatially distributed assets whose importance to service functionality varies across the network. This challenge is particularly acute in volcanic regions, where infrastructure may be exposed to hazards from multiple volcanoes with different eruption frequencies and impact footprints. This makes it hard to know where to focus resources for response, recovery and resilience planning ahead of an event. Here we present a probabilistic disruption scoring framework that combines hazard intensity, spatial extent, and occurrence probability with infrastructure exposure, asset criticality, and vulnerability to quantify the relative disruption potential of different hazard sources and locations. Asset criticality is represented by the number of people served, enabling impacts on individual infrastructure assets to be translated into a common disruption metric. We apply the framework to mainland Japan to assess potential electricity disruptions from tephra fall, considering impacts on power plants, transmission towers and substations exposed to simulated tephra fall events from 62 active volcanoes. A disruption score was calculated for each hazard footprint and used to rank the disruption potential of different tephra fall events and source volcanoes. We also quantified the contribution of different spatial areas to the annual expected electricity disruption across mainland Japan to identify locations with high disruption potential and disruption hotspots. Conditional on an eruption occurring, Fujisan is the volcano with the highest disruption potential because of its proximity to Tokyo and high criticality electricity infrastructure in central Japan. When eruption probabilities are incorporated, Asamayama emerges as the largest contributor to annual expected electricity disruption. Disruption hotspots are concentrated in major metropolitan centres, including Tokyo, Osaka, and Nagoya, as well as regions containing high criticality electricity generation facilities such as Tohoku. These findings provide a quantitative basis for prioritising volcanic risk reduction and infrastructure resilience measures. As the framework uses open-source globally available datasets and models, it can be readily applied to other hazards, infrastructure sectors, and geographic regions, providing a scalable screening tool for identifying priority hazard sources, locations, and infrastructure assets where more detailed risk and resilience investigations are likely to be most beneficial.

https://doi.org/10.5194/egusphere-2026-5468
Preprint. Discussion started: 11 September 2026
© Author(s) 2026. CC BY 4.0 License.

1 Introduction

Critical infrastructure systems deliver essential services, such as electricity, communications and transportation, that underpin the functioning of society and the economy (UNDRR, 2020). Natural hazards like floods, earthquakes and volcanic eruptions affect the performance of critical infrastructure in various ways, for example by causing direct damage to infrastructure assets, downtime during cleanup operations, increased maintenance requirements, and long-term degradation (G. Wilson et al., 2014; Nirandjan et al., 2024; Cha et al., 2025). As many critical infrastructure systems comprise networks of interdependent and spatially distributed assets, localised impacts can propagate through the system and affect service delivery across much larger regions (Rinaldi et al., 2001; Helbing, 2013; Pescaroli and Alexander, 2015; Mühlhofer et al., 2024). Disruption to infrastructure systems therefore depends not only on the severity of hazard impacts but also on which assets are affected and the role those assets play in maintaining service functionality. Identifying the assets, locations, and hazard sources most likely to generate widespread disruption is consequently an important challenge for risk assessment, resilience planning, and disaster risk reduction (Hallegatte et al., 2019).

Quantifying disruption within distributed critical infrastructure systems requires understanding how localised natural hazard impacts to individual assets can affect service delivery across the broader infrastructure network. Detailed network models can represent infrastructure interdependencies and assess the consequences of asset failures for system performance (Ouyang, 2014). However, the data required for such models are often not available or easily accessible (Schotten et al., 2024). These approaches are also typically data- and compute-intensive which limit their applicability across large geographic areas and multiple hazard sources (Eidsvig et al., 2017). As a result, decision-makers often lack efficient methods for identifying which hazards and locations should be prioritised for more detailed investigation. To address this, several studies have proposed scoring-based approaches that incorporate measures of infrastructure criticality to rapidly assess disruption potential and identify areas where more detailed analyses may be warranted. For example, Eidsvig et al. (2017) developed an indicator-based framework that includes the number of users and downtime of infrastructure to rank hazard scenarios affecting infrastructure at a specific site. Hayes et al. (2022a) developed a Road Segment Disruption Score that combined hazard impacts and road criticality to identify disruption-prone road segments during a volcanic eruption. Such approaches become particularly useful when coupled with prioritisation tools such as risk ranking and hotspot analysis techniques that support the prioritisation of limited resources for mitigation and resilience planning (Dilley et al., 2005; Fischhoff and Morgan, 2013; Thacker et al., 2017).

The challenge of prioritisation becomes more complex when infrastructure assets within distributed systems are exposed to hazards from multiple potential sources. Dense volcanic regions such as Indonesia, Japan, and Central America contain many active volcanoes, each capable of generating a variety of hazards with different spatial footprints, frequencies, and impact intensities (Alberico et al., 2011; Biass et al., 2014; Jenkins et al., 2022). Consequently, a single infrastructure asset may be

https://doi.org/10.5194/egusphere-2026-5468
Preprint. Discussion started: 11 September 2026
© Author(s) 2026. CC BY 4.0 License.

exposed to hazards originating from multiple volcanoes, making it difficult to determine which hazard sources contribute most to disruption risk. This is particularly relevant for tephra fall because it is the most frequent and widespread volcanic hazard and can affect areas extending hundreds to thousands of kilometres from the source volcano (Jenkins et al., 2015), making it a common cause of critical infrastructure disruption during volcanic eruptions.

Electricity networks are among the infrastructure systems most vulnerable to tephra fall impacts and are particularly important because many other infrastructure systems depend on electricity to maintain service delivery (Nicolas et al., 2019). Tephra fall can disrupt power generation, transformation, transmission and distribution through various mechanisms (T. Wilson et al., 2012). The most frequently observed effect is tephra-induced flashover whereby even a fine coating of 1–3 mm of damp or wet tephra can cause leakage current and short-circuiting across station and line insulators (Wardman et al., 2014; Homma et al., 2019). Another common impact is damage to moving mechanical components, for example wind and/or water turbines at electricity generation sites, caused by the abrasive properties of tephra (Wardman et al., 2012; T. Wilson et al., 2012; G. Wilson et al., 2014). Tephra can also force the de-energising of equipment to remove tephra, potentially requiring system operators to reroute power through other portions of the network or initiate rolling outages (Wardman et al., 2012; T. Wilson et al., 2012). The severity and spatial extent of disruption depend not only on the tephra fall distribution and frequency from a source volcano but also on the location and criticality of the infrastructure affected. Identifying the volcanoes and locations with the highest disruption potential could therefore support more targeted resilience planning and risk reduction efforts.

In this study, we present a disruption scoring framework to quantify the relative disruption potential for different hazard sources and locations to identify those with the highest potential to disrupt critical infrastructure systems. The framework assesses both the severity and likelihood of disruption, combining the degree and frequency of hazard impacts with infrastructure asset location and criticality which is quantified here as the number of people served. We combine simulated hazard footprints, capturing hazard intensity and spatial extent, with vulnerability and criticality measures for each asset to calculate disruption scores, which we then use to compare hazard footprints, hazard sources and spatial areas through risk ranking and hotspot analysis. We apply this framework to mainland Japan (Hokkaido, Honshu, Shikoku and Kyushu) to assess potential electricity disruption from tephra fall. Japan was selected for its dense electricity network and 62 active mainland volcanoes with confirmed Holocene eruptions potentially capable of causing considerable impacts to society (Fujita et al., 2020). We rank these volcanoes by disruption potential, identify disruption hotspots across mainland Japan, and benchmark two historical eruptions (the 2011 Shinmoedake eruption at Kirishimayama and the 1707 Hoei eruption at Fujisan) against the range of disruption produced from our simulated eruptions.

https://doi.org/10.5194/egusphere-2026-5468
Preprint. Discussion started: 11 September 2026
© Author(s) 2026. CC BY 4.0 License.

2 Methods

2.1 Overview of disruption scoring framework

Our disruption scoring framework builds on the hazard-exposure-vulnerability approach commonly used to assess disaster risk (UNDRR, 2015), adding an asset criticality component that captures each asset's varying importance to the system's overall functionality and service delivery. Asset criticality is quantified by the number of people served, reflecting the population that would potentially experience disruptions if the asset was impacted (Thacker et al., 2014; Thacker et al., 2017). The framework consists of four main steps, with details for each provided in the following sections:

1) Assigning criticality to each infrastructure asset within the system (Sect. 2.2)
2) Selecting hazard sources and generating probabilistic hazard footprints (Sect. 2.3)
3) Determining the annual probability of occurrence for each hazard event (Sect. 2.4)
4) Calculating disruption scores and disruption potential metrics (Sect. 2.5)

Figure 1 provides an overview of the framework in the context of its application to mainland Japan to assess potential electricity disruption resulting from tephra fall. Hazard footprints are combined with infrastructure vulnerability and criticality information to calculate disruption scores for individual assets and hazard scenarios. These scores are subsequently aggregated to quantify the relative disruption potential of different volcanoes and locations, enabling the identification of priority hazard sources and disruption hotspots.

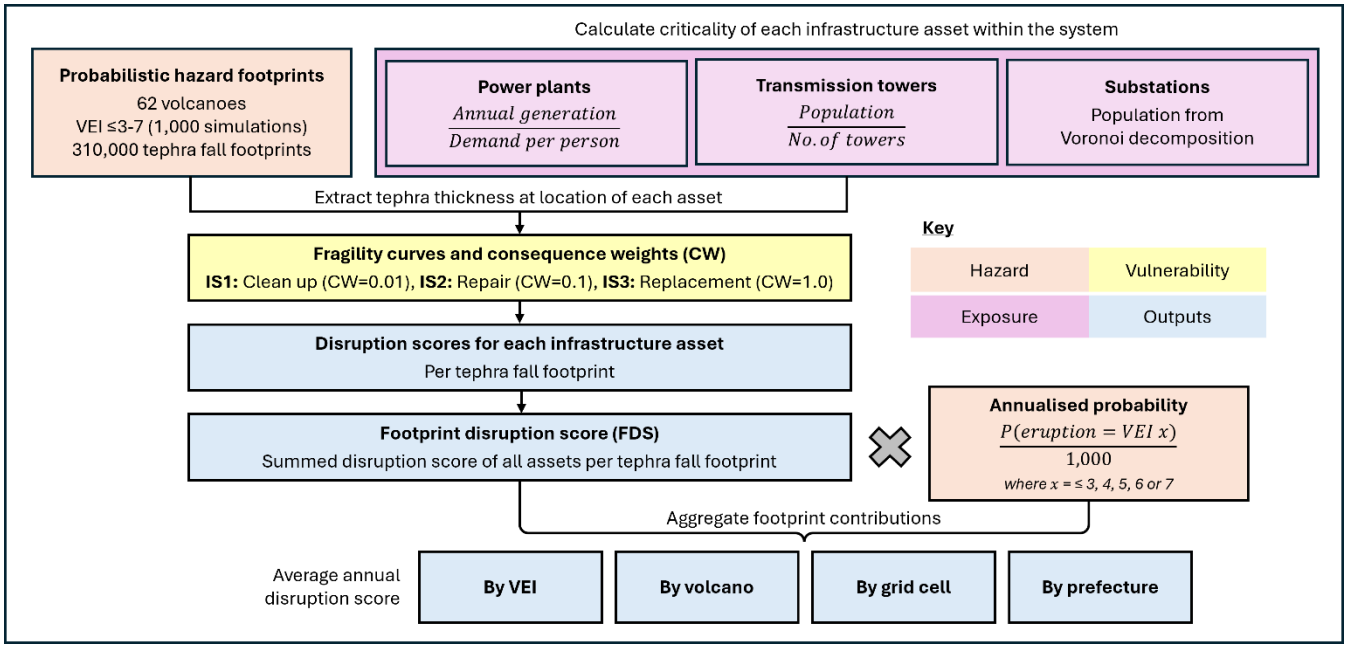

https://doi.org/10.5194/egusphere-2026-5468
Preprint. Discussion started: 11 September 2026
© Author(s) 2026. CC BY 4.0 License.

Figure 1: Overview of the disruption scoring framework developed for distributed critical infrastructure systems to quantify relative disruption potential of multiple hazard sources and spatial areas. The framework is illustrated through its application to mainland Japan to assess potential electricity disruption due to tephra fall impacts on electricity infrastructure. Probabilistic hazard modelling is used to generate tephra fall footprints across five VEI classes (≤ 3, 4, 5, 6 and 7) for 62 volcanoes, which are combined with asset vulnerability and criticality information to calculate disruption scores for individual assets and subsequently, for each hazard footprint. Footprint disruption scores are weighted by their annual probability of occurrence and aggregated to quantify the contributions of hazard sources and spatial areas to the overall average annual disruption score for mainland Japan. Abbreviations: VEI - volcanic explosivity index; CW - consequence weight; IS - impact state; FDS - footprint disruption score.

2.2 Assigning criticality to electricity infrastructure assets

2.2.1 Datasets

The electricity network was represented using three asset types corresponding to the main stages of electricity supply: power plants (generation), transmission towers (transmission), and substations (transformation and distribution). Power plant locations and attributes were obtained from the Global Power Plant Database (Byers et al., 2021). To account for plant closures following the 2011 Fukushima Daiichi event, we cross-checked the database against the World Nuclear Association's reactor database (as of December 2025) and removed those now permanently shut down (n=1). Transmission tower and substation locations were extracted from OpenStreetMap with the key-value pairs *power=tower* and *power=substation* (OpenStreetMap contributors, 2025). Population estimates were obtained from the WorldPop Japan 2024 Population Counts dataset (100m resolution; Bondarenko et al., 2025). Electricity demand data for the fiscal year 2024 (April 2024 – March 2025) were sourced from reports published by the Organization for Cross-regional Coordination of Transmission Operators (OCCTO, 2025).

2.2.2 Estimating the number of people served

Asset criticality was quantified as the estimated number of people served by each electricity infrastructure asset. In the absence of detailed asset ownership and power flow data, criticality was defined relative to the regional electricity service area in which each asset is located. This assumption is consistent with the organisation of Japan's electricity network, where electricity supply is primarily managed within nine regional service areas, although interconnections between regions allow some power exchange (Uehara and Ikeda, 2016; IEA, 2022; OCCTO, 2025). Table 1 summarises the population and electricity infrastructure assets within each service area.

https://doi.org/10.5194/egusphere-2026-5468
Preprint. Discussion started: 11 September 2026
© Author(s) 2026. CC BY 4.0 License.

Service Area	Population	Power Plants	Total Annual Generation / GWh	Transmission Towers	Substations
Chubu	15,530,809	61	139,456	34,074	616
Chugoku	7,160,283	39	47,476	20,326	299
Hokkaido	5,184,964	42	35,060	30,265	386
Hokuriku	2,833,043	15	49,980	10,769	213
Kansai	20,197,220	55	153,752	24,042	672
Kyushu	12,282,941	101	115,754	25,470	596
Shikoku	3,565,126	24	47,848	8,781	178
Kanto	44,710,352	87	175,481	41,326	1,610
Tohoku	10,668,256	90	191,564	49,063	933
Total	**122,132,993**	**514**	**956,371**	**244,116**	**5,503**

Table 1: Population and number of electricity infrastructure assets by asset type for each regional service area in mainland Japan. The total annual generation of power plants within each service area is also included (from estimates for 2017; Byers et al., 2021). Population estimates are for 2024 (WorldPop; Bondarenko et al., 2025). Transmission tower and substation counts are based on OpenStreetMap data as of June 2025 (OpenStreetMap contributors, 2025).

The method used to estimate the number of people served differs by asset type. For power plants, criticality was based on the estimated electricity demand that each plant could fulfil. The average annual electricity demand per person (GWh/person; for FY2024) was calculated within each service area using annual electricity demand and population data (Bondarenko et al., 2025; OCCTO, 2025). The estimated annual generation (GWh) of each power plant (Byers et al. 2021) was then divided by the corresponding per capita demand to estimate the number of people a power plant could serve.

Transmission towers typically carry insulators and are essential for power transmission, supporting power lines that transport electricity across an area. The same criticality was assigned to all transmission towers within the same service area. The criticality is calculated as the service area population divided by the total number of transmission towers. This approach reflects the assumption that transmission assets serving larger populations are more critical, while networks containing more towers offer greater redundancy and alternative pathways for power transfer, reducing the relative criticality of individual towers.

Substations are responsible for transforming electricity to appropriate voltage levels for transmission and distribution to end-users. We determined the criticality of each substation using Voronoi decomposition following Thacker et al. (2014). Voronoi polygons were generated around each substation to approximate the area it served, assuming that each substation served the area closest to it (irrespective of regional service area boundaries). The population contained within each polygon was then calculated using zonal statistics and used as a proxy for the number of people served. Although this approach does not account for operational characteristics such as voltage levels or power flow directions, it provides a practical approximation of substation criticality using publicly available data.

https://doi.org/10.5194/egusphere-2026-5468
Preprint. Discussion started: 11 September 2026
© Author(s) 2026. CC BY 4.0 License.

2.3 Selecting volcanoes and probabilistic tephra fall modelling

We assessed the disruption potential of active volcanoes on mainland Japan. Offshore and submarine volcanoes were excluded as they are unlikely to contribute substantially to tephra fall impacts on electricity infrastructure assets on mainland Japan. Volcanoes were selected from the Global Volcanism Program's (GVP) Holocene Volcano List (GVP, 2025; volcanoes in this study are referred to using the names provided in the list) based on the following criteria:

i. Volcano has a country classification of "Japan" within the GVP Holocene Volcano List (n=105);
ii. Volcano is located on mainland Japan i.e. Hokkaido, Honshu, Shikoku and Kyushu (n=67); and
iii. Volcano has a confirmed Holocene eruption (n=62)

Application of these criteria resulted in a final set of 62 volcanoes (Honshu=39; Hokkaido=15; Kyushu=8; Shikoku=0). Potential tephra fall footprints were generated using TephraProb, which employs the Tephra2 model to probabilistically simulate tephra dispersion and deposition (Bonadonna et al., 2005; Biass et al., 2016). We simulated 1,000 eruptions for each of five eruption intensity classes, represented by the Volcanic Explosivity Index (VEI ≤ 3, 4, 5, 6 and 7; Newhall and Self, 1982), using a range of eruption source parameters and wind conditions (Supplementary Material A). Tephra deposition was modelled on a 1 × 1 km grid extending 1,000 km from the volcano and expressed as tephra thickness, calculated from deposited mass assuming a bulk density of 1,000 kg m^{-3}. Wind conditions were stochastically sampled from the European Centre for Medium Range Weather Forecasts (ECMWF) ERA5 dataset (Hersbach et al., 2023) over a ten-year period (6-hour interval; 2015–2024). To enable a national-scale analysis while maintaining computational efficiency, tephra fall simulations were performed for Fujisan using local wind conditions and subsequently spatially repositioned to each of the other 61 study volcanoes. This approach was adopted because wind profiles across mainland Japan exhibit broadly similar characteristics, with prevailing eastward transport dominating much of the atmospheric column throughout the year (Fig. 2). Although regional and seasonal variations exist, they are comparatively small relative to the scale of this assessment. The resulting dataset comprises 310,000 simulated tephra fall footprints (62 volcanoes × 5 VEI classes × 1,000 simulations).

https://doi.org/10.5194/egusphere-2026-5468
Preprint. Discussion started: 11 September 2026
© Author(s) 2026. CC BY 4.0 License.

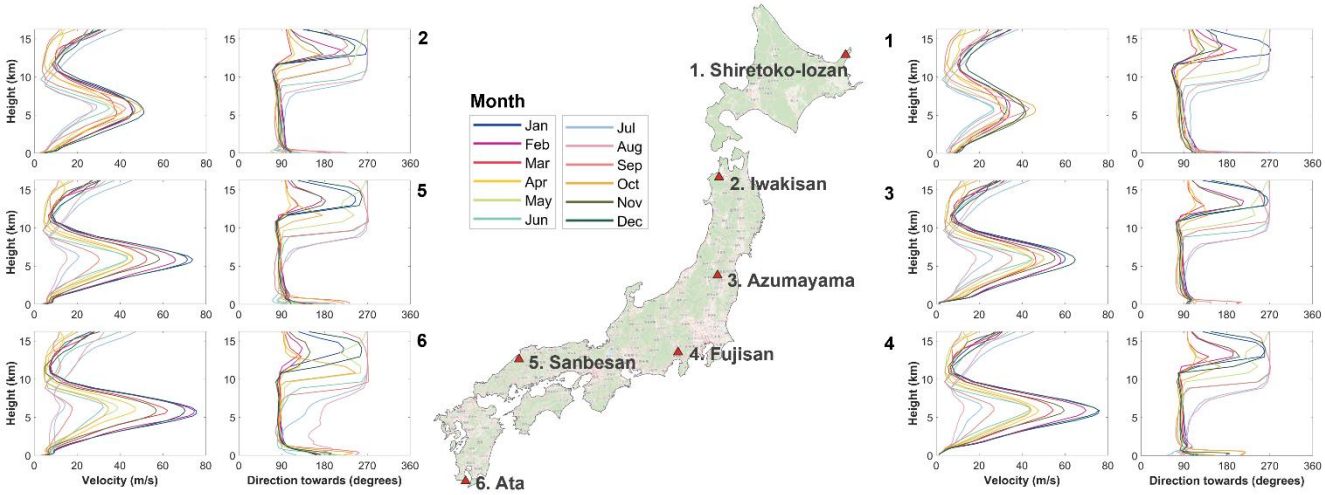

Figure 2: Monthly wind profiles (median wind velocity and direction wind blows towards) for selected volcanoes showing relatively minor differences across mainland Japan. As such, this study uses the wind profile of Fujisan across all volcanoes for the purpose of reducing simulation runtimes. Wind data are from the European Centre for Medium Range Weather Forecasts (ECMWF) ERA5 dataset (Hersbach et al., 2023) over a ten-year period (6-hour interval; 2015–2024). Base map: © OpenStreetMap contributors

2.4 Determining annual probability of occurrence

To account for differences in eruption frequency among volcanoes and eruption VEIs, annual probabilities were estimated for VEI ≤3–7 eruptions at each of the 62 study volcanoes. Probabilities were calculated following the methodology of Jenkins et al. (2018), which explicitly accounts for incompleteness in the historical eruption record. The annual probability of an eruption with a specific VEI was estimated as the product of two components: i) the annual probability of any eruption occurring at a volcano, and ii) the conditional probability that the eruption is of a particular VEI class (Hayes et al., 2022b). The annual probability of any eruption was calculated from volcano-specific eruption records (Jenkins et al., 2012). Where sufficient eruption records existed, volcano-specific data were also used to constrain the relative occurrence of small (VEI ≤ 3) and large (VEI ≥ 4) eruptions before calculating VEI-specific probabilities for VEI 4–7 using global analogue volcano datasets following Jenkins et al. (2012, 2018). The resulting annual eruption probabilities were used to weight the disruption scores associated with each simulated tephra fall footprint (Sect. 2.5). Eruption probabilities for all volcanoes and VEI classes are provided in Supplementary Material B.

2.5 Calculating disruption scores and disruption potential metrics

2.5.1 Calculating footprint disruption scores (FDS)

Disruption scores were calculated for each electricity infrastructure asset by combining hazard exposure, asset vulnerability, and asset criticality. For each simulated tephra fall footprint, the tephra thickness at the location of each asset was extracted and used to estimate the probability of the asset reaching different impact states. Fragility functions based on those developed

https://doi.org/10.5194/egusphere-2026-5468
Preprint. Discussion started: 11 September 2026
© Author(s) 2026. CC BY 4.0 License.

by G. Wilson et al. (2017) for electricity infrastructure exposed to tephra fall (Fig. 3) were used to derive the probability of an asset being in each of the three impact states (IS): IS1 (cleanup required), IS2 (repair required), and IS3 (replacement required).

To translate physical impacts into service disruption, each impact state was assigned a consequence weight representing the relative severity of disruption associated with that state. The consequence weights, which are heuristic severity weights rather than empirically estimated fractions of customers experiencing disruption, were assigned as 0.01 (IS1), 0.1 (IS2), and 1.0 (IS3). These weights reflect the expectation that disruption severity increases non-linearly with damage severity (He and Cha, 2018) and recognise that infrastructure systems often contain operational and engineering measures that reduce the impacts of minor failures, such as network redundancy, fault isolation, and service rerouting (Bruneau et al., 2003; Mottahedi et al., 2021; Zhao et al., 2025). Consistent with G. Wilson et al. (2014), IS1 and IS2 were assumed to represent predominantly temporary disruptions, whereas IS3 was assumed to result in widespread disruption affecting all users served by the asset. Sensitivity testing using an alternative set of consequence weights (0.25, 0.50, and 0.75 for IS1–IS3, respectively) produced only minor changes in the ranking of volcanoes and locations, indicating that the results are not strongly dependent on the selected weights.

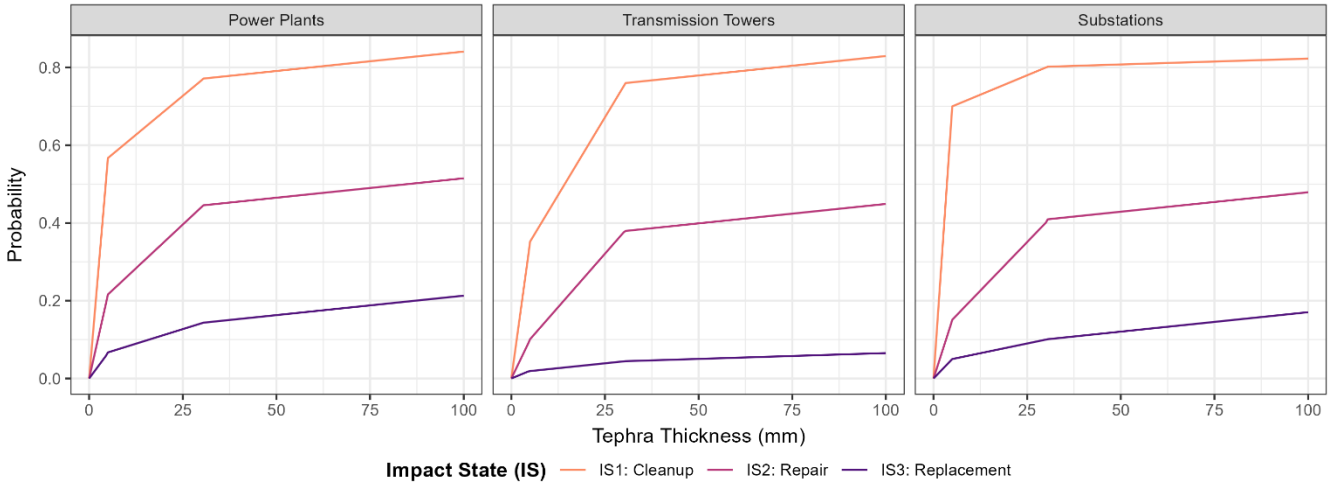

Figure 3: Fragility curves for each electricity asset type, showing the probability of an infrastructure asset being in or exceeding the three impact states for a given tephra thickness (0–100 mm shown). The fragility curves are based on those developed by G. Wilson et al. (2017) for mixed generation type, transmission lines and substations, which were derived using post-eruption impact assessments (electricity generation = 12; transmission lines = 24; substations = 16) and expert judgement. Fragility curves were used to calculate the probability of an asset being in each of the three impact states for the simulated tephra thickness at its location.

The disruption score *DS* for each electricity infrastructure asset e in grid cell g of a tephra fall footprint f from volcano v was calculated according to Eq. (1) below:

$$DS_{e,f,v} = CR_e \times \sum_{i=1}^{3} P(IS_e = i \mid T_{g(e),f,v}) \times CW_i \,, \tag{1}$$

https://doi.org/10.5194/egusphere-2026-5468
Preprint. Discussion started: 11 September 2026
© Author(s) 2026. CC BY 4.0 License.

where CR represents asset criticality in terms of number of people served (Sect. 2.2). The summation expression, $\sum_{i=1}^{3} P(IS_e = i \mid T_{g(e),f,v}) \times CW_i$, is the probability of the asset being in impact state i given tephra thickness T, multiplied by the consequence weight CW for the impact state. The footprint disruption score (FDS) for a simulated tephra fall footprint was then calculated by summing the disruption scores of all exposed assets, as given by Eq. (2):

$$FDS_{f,v} = \sum_e DS_{e,f,v} \quad (2)$$

The FDS therefore represents the total disruption score associated with a given hazard footprint. Asset disruption scores can also be aggregated within any spatial unit (e.g. grid cell or prefecture) to support spatial analysis.

To account for differences in eruption frequency among volcanoes and VEI classes, each FDS can also be weighted (i.e. multiplied) by its annual probability of occurrence $P_{f,v}$. The probability assigned to an individual tephra fall footprint was calculated by dividing the annual probability of an eruption of the corresponding VEI class at the source volcano by the number of simulated footprints for that VEI (i.e. 1,000). As wind conditions were stochastically sampled during the hazard simulations, all footprints within a given volcano–VEI combination were assumed to be equally likely. For comparison and ranking purposes, both unweighted and probability-weighted FDS values were normalised independently to a scale of 0–100.

2.5.2 Calculating disruption potential metrics

Probability-weighted footprint disruption scores represent the average annual contribution of individual tephra fall footprints to the average annual electricity disruption across mainland Japan. Summing probability-weighted FDS values across multiple footprints provides the average annual disruption score (AADS) for any selected grouping, such as a volcano, VEI class, grid cell, or prefecture, as in Eq. (3):

$$AADS_x = \sum_{(f,v) \in x} FDS_{f,v} \times P_{f,v} \text{ , where } x \text{ denotes any selected grouping of tephra fall footprints} \quad (3)$$

The AADS was used to quantify and compare the relative contribution of different hazard sources and locations to annual expected electricity disruption. In addition, exceedance probability (EP) curves were constructed by ranking FDS values from largest to smallest and cumulatively summing their annual probabilities of occurrence. These curves describe the annual probability of equalling or exceeding a given disruption score.

To identify areas that disproportionately contribute to annual expected electricity disruption, hotspot analysis was performed using the AADS calculated for each 5 x 5 km grid cell across mainland Japan. We used a grid resolution coarser than that used for the tephra dispersal modelling to reduce computational time while providing sufficient spatial detail to distinguish disruption hotspots. The Getis-Ord Gi* statistic (Getis and Ord, 1992) was used to identify statistically significant clusters of high AADS values (with 90 % confidence), thereby highlighting disruption hotspots within mainland Japan's electricity network.

https://doi.org/10.5194/egusphere-2026-5468
Preprint. Discussion started: 11 September 2026
© Author(s) 2026. CC BY 4.0 License.

2.5.3 Calculating historical eruption disruption scores

To place the simulated disruption scores in context, the disruption scoring framework was applied to two historical eruptions: the 2011 Shinmoedake eruption at Kirishimayama and the 1707 Hoei eruption at Fujisan. The Shinmoedake eruption was selected because its impacts on the electricity network are well documented (Magill et al., 2013), while the Hoei eruption is a commonly cited scenario anticipated to cause large-scale tephra fall impacts were it to occur today (Yamamoto and Nakada, 2015; Fujita et al., 2020; Suzuki, 2018).

For each event, we overlaid electricity infrastructure assets with the corresponding tephra fall isopach maps (Magill et al., 2013, for the 2011 Shinmoedake eruption; Miyaji et al., 2011, for the 1707 Hoei eruption) to calculate FDS values. As isopach maps represent deposition as thickness intervals rather than continuous values, two FDS estimates were calculated for each eruption. The first used the lower bound of the tephra thickness interval associated with each asset, while the second used the upper bound. For assets located within the maximum thickness isopach, where no upper bound exists, the lower bound value was used. These calculations provide a plausible range of FDS values for each historical eruption, helping to contextualise the distribution of disruption scores from simulated eruptions of similar intensities by comparing them with known events.

3 Results

3.1 Spatial distribution of criticality

The criticality of electricity infrastructure assets is concentrated in the major urbanised coastal regions of mainland Japan, particularly around the Tokyo, Osaka, and Nagoya metropolitan areas (Fig. 4). This pattern reflects the concentration of population and electricity demand within the coastal plains of central Japan. Power plants exhibit substantially higher criticality than transmission towers and substations. The power plant with the maximum asset criticality serves approximately eight million people, compared with 296,000 for the substation, and 1,081 for the transmission tower with the highest criticality. Unlike substations and transmission towers, whose criticality generally follows population distribution (Fig. 4b-c), high criticality power plants are more geographically distributed across mainland Japan (Fig. 4a). Some of the highest criticality power plants are located along the coasts of Fukushima, Miyagi and Niigata prefectures, away from major population centres. This reflects the fact that power plant locations are determined not only by demand, but also by factors such as generation type, resource availability, site suitability, and development costs (Suzuki, 2018). Consequently, the spatial distribution of disruption potential is expected to be shaped by two contrasting patterns: concentrated criticality associated with urban electricity demand and dispersed criticality associated with major power generation facilities.

https://doi.org/10.5194/egusphere-2026-5468
Preprint. Discussion started: 11 September 2026
© Author(s) 2026. CC BY 4.0 License.

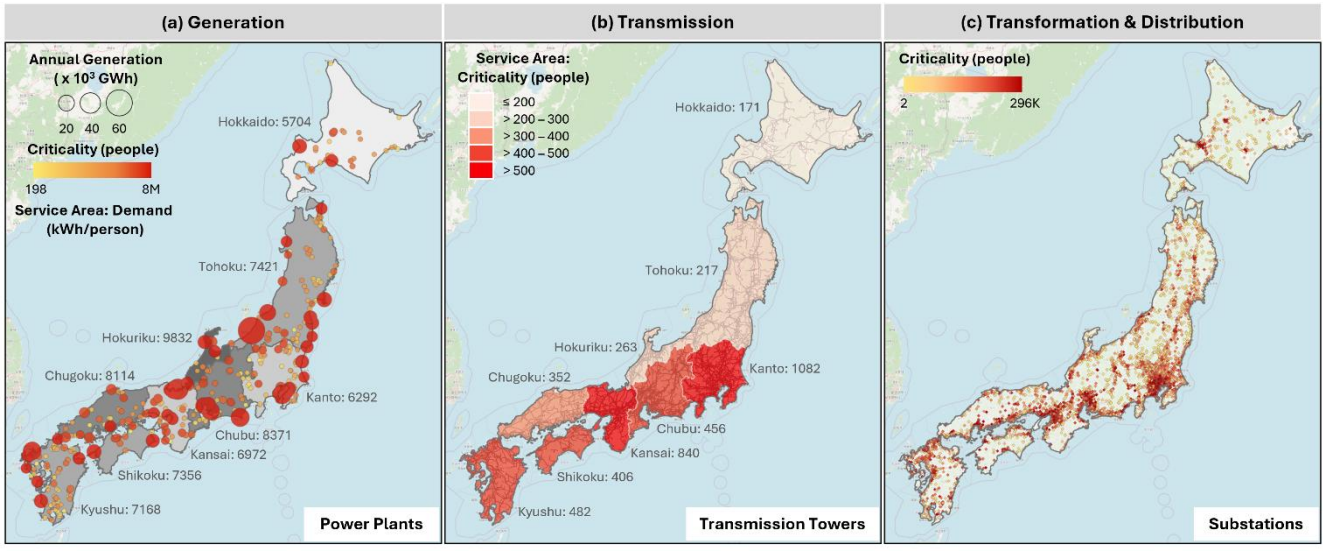

Figure 4: Spatial distribution of the criticality of electricity infrastructure assets, represented by the estimated number of people the infrastructure serves. (a) The criticality of power plants, indicated by the colour of the points, is obtained by dividing the estimated annual generation of the plant for 2017 (represented by size; Byers et al., 2021) by the annual demand per person for each service area (grey scale, labelled). (b) The location of the transmission towers is shown as grey dots and those towers within the same service area have the same criticality (labelled), given by the average number of people per tower for the service area. (c) The criticality for substations, represented by the diamond points, is estimated using Voronoi decomposition (Thacker et al., 2014). Base map: © OpenStreetMap contributors

3.2 Footprint disruption scores (FDS)

3.2.1 By VEI

Most simulated tephra fall footprints produced some level of electricity disruption, with fewer than 3 % (n=8,093) having an FDS of zero. Of these non-disruptive footprints, the vast majority (~80 %) are from smaller eruptions (VEI ≤3–4) and nearly 50 % originate from just two volcanoes, Shiretoko-Iozan and Rausudake.

Both the unweighted and probability-weighted FDS distributions are strongly positively skewed (Fig. 5), indicating that severe disruption scenarios are possible but not common. Most simulated eruptions produce disruption scores in the lowest FDS bin (0–10), whereas only a small proportion generate large electricity disruption. For the unweighted FDS, where all simulated footprints are considered equally likely regardless of the source volcano and eruption VEI, larger VEI classes are increasingly dominant at larger disruption scores, reflecting their ability to generate more spatially extensive and thicker tephra falls, whereas the proportion from smaller VEI classes decreases (Fig. 5a, 5d). However, this trend is not observed for the probability-weighted FDS because smaller eruptions are more frequent, thus they contribute more to annual expected electricity disruption than rarer, larger eruptions (Fig. 5b). Consequently, the maximum probability-weighted FDS for a VEI 7 footprint is smaller than that for a VEI ≤ 3 footprint, and the highest probability-weighted FDS bins contain only VEI ≤ 3 footprints (Fig. 5f).

https://doi.org/10.5194/egusphere-2026-5468
Preprint. Discussion started: 11 September 2026
© Author(s) 2026. CC BY 4.0 License.

Volcanoes associated with the largest disruption scores differ depending on whether disruption severity alone or eruption frequency is considered. The largest unweighted FDS are generated by volcanoes located near the Tokyo Metropolitan Area, including Hakoneyama (VEI ≤3–5), Harunasan (VEI 6), and Izu-Tobu (VEI 7). In contrast, the largest probability-weighted FDS values are produced by volcanoes more broadly distributed across central Japan, including Asamayama (VEI ≤ 3), Fujisan (VEI 4), Azumayama (VEI 5), and Aira (VEI 6–7). This highlights the importance of considering both disruption severity and eruption frequency when assessing disruption potential.

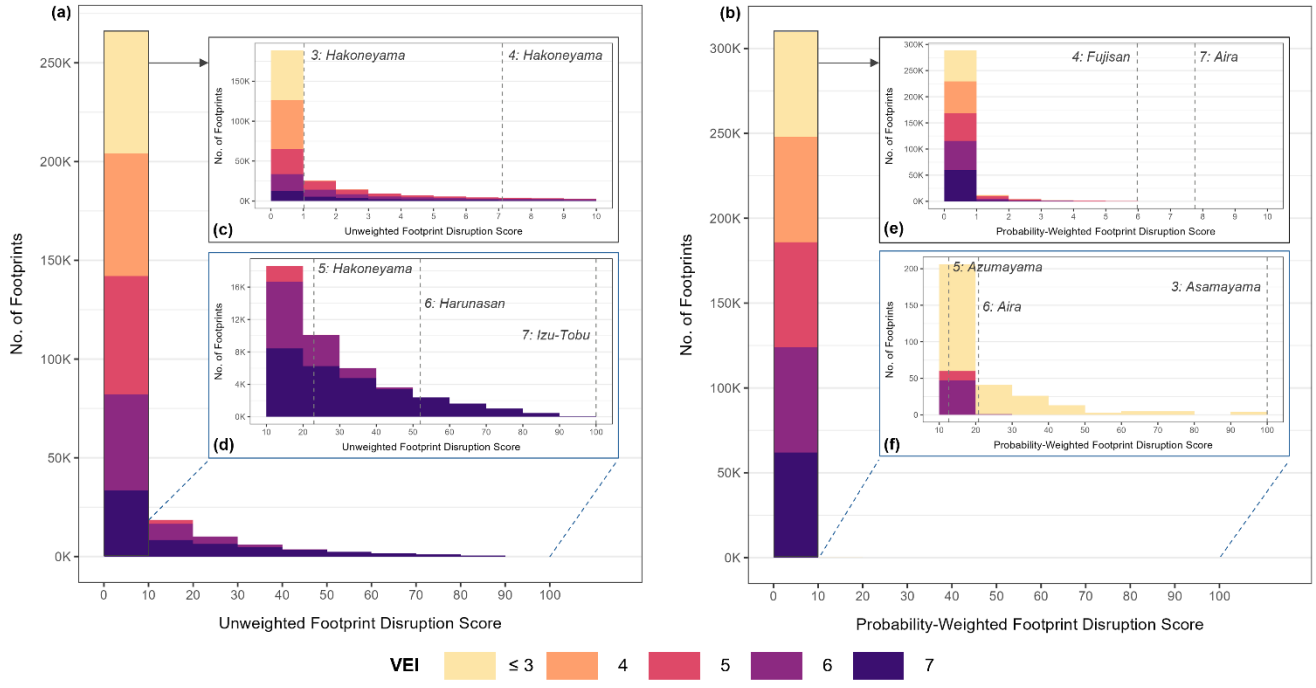

Figure 5: Histograms of (a) unweighted and (b) probability-weighted footprint disruption scores (FDS), normalised to a scale of 0-100, for all simulated tephra fall footprints from 62 active volcanoes on mainland Japan. For each volcano, 1,000 footprints were simulated for each VEI class. Insets show the histograms zoomed-in on specific FDS ranges: (c) and (e) for FDS 0–10, and (d) and (f) for FDS 10–100. Vertical dashed lines indicate the maximum FDS for each VEI class, with the corresponding volcano labelled. The minimum FDS for all VEI classes falls within the lowest bin (FDS = 0–10).

3.2.2 By month

Footprint disruption scores (FDS) exhibit only weak seasonal variability (Fig. 6; for Fujisan only as the wind conditions at other volcanoes are approximated). Neither the unweighted nor probability-weighted median FDS show a distinct seasonal peak, despite clear seasonal fluctuations in electricity demand, which peaks in winter (January) and summer (July–August) (Fig. 6a). Median unweighted FDS values are marginally higher during summer (Fig. 6b), whereas median probability-weighted FDS values are slightly higher during autumn and winter (Fig. 6c). Seasonal differences are most apparent in the variability of the unweighted FDS. The interquartile range increases through the first half of the year, peaks during summer,

https://doi.org/10.5194/egusphere-2026-5468
Preprint. Discussion started: 11 September 2026
© Author(s) 2026. CC BY 4.0 License.

and then declines towards winter (Fig. 6b), suggesting a broader range of potential disruption severities during the period where electricity demand is highest. Across the year, the FDS distributions remain positively skewed, indicating that small disruption scenarios are consistently more common than large disruption scenarios.

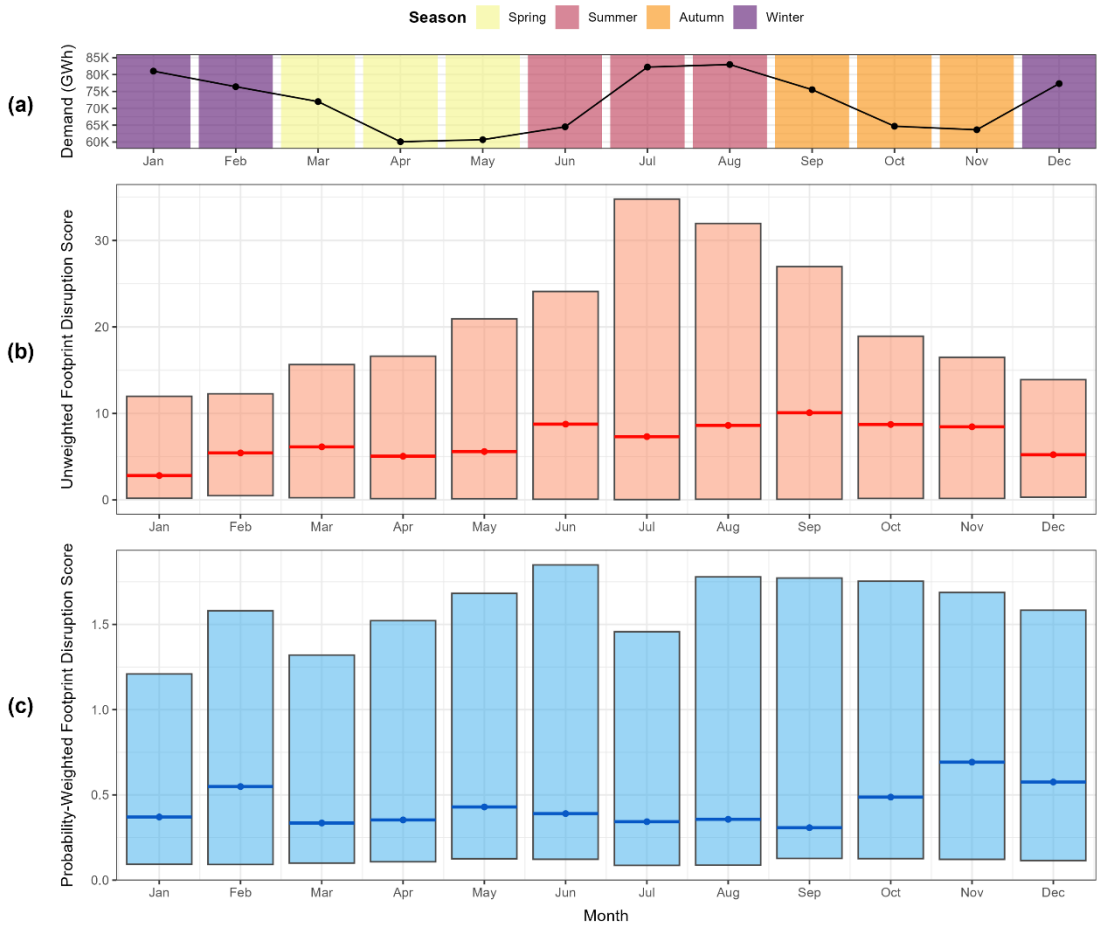

Figure 6: Comparison of (a) electricity demand for FY2024 (April 2024 –March 2025; OCCTO, 2025) with (b) unweighted and (c) probability-weighted footprint disruption scores (FDS) by month for Fujisan. Seasons follow the definition of the Japan Meteorological Agency. The boxplots show the median FDS (horizontal line with dot) and interquartile range (box bounded by the 25th and 75th percentiles) for tephra fall footprints simulated with wind data over a ten-year period (2015–2024). Note: The unweighted and probability-weighted FDS are normalised independently to a scale of 0–100 and not comparable directly.

3.2.3 Exceedance probability (EP) curves

The exceedance probability (EP) curves demonstrate a strong trade-off between disruption severity and event frequency (Fig. 7). Small disruption scores are associated with comparatively high annual exceedance rates and are dominated by VEI ≤ 3 and 4 eruptions which are relatively frequent but generally of low disruption potential (Fig. 7b-c). On the other hand, large disruption scores occur only at low exceedance rates, indicating that progressively larger disruption scores are associated with

https://doi.org/10.5194/egusphere-2026-5468
Preprint. Discussion started: 11 September 2026
© Author(s) 2026. CC BY 4.0 License.

increasingly rarer events, primarily contributed by VEI 5–7 eruptions (Fig. 7d-f). At very low annual exceedance rates (< 10^{-6}), the EP curve becomes nearly vertical, suggesting that the FDS approaches an upper limit, with only small increases in FDS despite further decreases in annual exceedance rates.

Volcano-specific EP curves reveal how different volcanoes contribute to disruption risk at different exceedance rates (Fig. 7). The shape of each EP curve reflects the distribution of FDS and the annual eruption probability for that volcano. Volcanoes characterised by relatively frequent, small eruptions, such as Asamayama, dominate exceedance of lower disruption scores at higher annual exceedance rates (> 10^{-3}). By contrast, volcanoes capable of producing infrequent but highly disruptive eruptions, such as Asosan and Aira, become increasingly important at lower annual exceedance rates (< 10^{-5}). Differences in curve shape also indicate variation in the range of disruption outcomes that a volcano can generate. For example, Fujisan and Hakoneyama exhibit broader ranges of potential disruption for VEI 4 eruptions, and therefore more shallow curves, than Azumayama, Asamayama, and Unzendake (Fig. 7c). Overall, the EP curves show that frequent eruptions contribute most to annual expected disruption, whereas rare large eruptions dominate the upper tail of the disruption distribution.

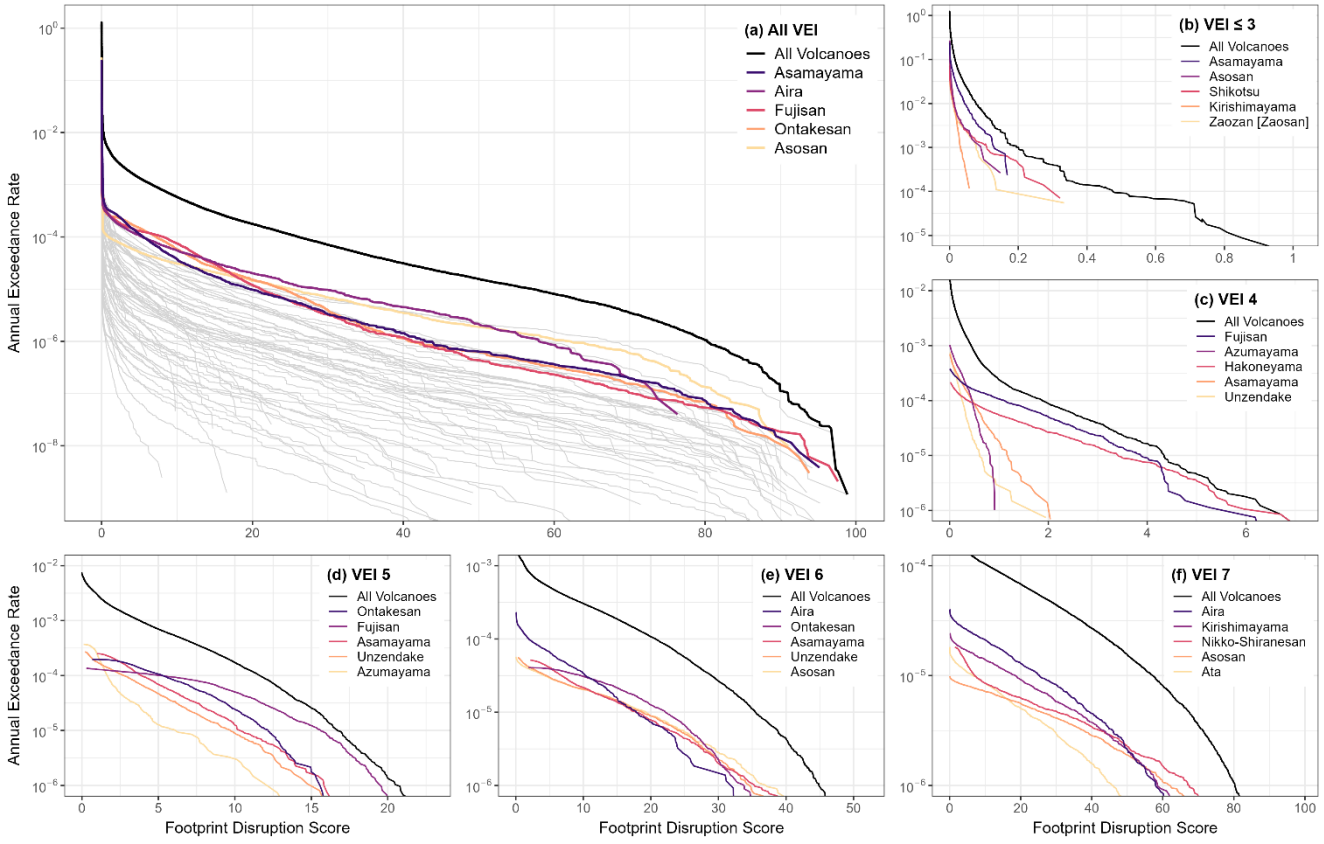

https://doi.org/10.5194/egusphere-2026-5468
Preprint. Discussion started: 11 September 2026
© Author(s) 2026. CC BY 4.0 License.

Figure 7: Exceedance probability (EP) curves showing the annual exceedance rate (AER) for equalling or exceeding a given footprint disruption scores (FDS) for (a) all simulated tephra fall footprints and (b-f) individual VEI classes (VEI ≤3–7). The coloured curves represent the five volcanoes with the largest contributions to annual expected electricity disruption for mainland Japan (All VEI) and within each VEI class. Individual volcanoes are listed in the legend in descending order of contribution, starting with the largest contributor. The grey curves in (a) show the EP curves for all other volcanoes. Note: Axes limits are different in each plot.

3.2.4 Volcano risk rankings

Volcano rankings differ markedly depending on whether disruption severity alone or both disruption severity and eruption frequency are considered (Fig. 8). Most volcanoes have unweighted FDS spanning multiple decile bins, demonstrating the variability in disruption severity that can be produced by a single volcano. However, individual decile bins are typically dominated by a relatively small number of volcanoes. The three volcanoes with the largest median unweighted FDS are Fujisan, Ontakesan and Sanbesan, accounting for 14 % of the footprints in the highest decile bin (Fig. 8a). These volcanoes are capable of generating some of the most disruptive tephra fall scenarios affecting Japan's electricity infrastructure.

Incorporating eruption frequency substantially changes these rankings. Asamayama becomes the largest contributor to annual expected electricity disruption, followed by Aira and Fujisan (Fig. 8b). Specifically, VEI ≤ 3 eruptions at Asamayama, followed by VEI 5 eruptions at Ontakesan and Fujisan have the largest average annual disruption scores (AADS). These results demonstrate that volcanoes capable of generating the most severe disruptions are not necessarily those that contribute most to long-term disruption risk. This influence of eruption frequency is substantial, with the median change in ranking being 15 positions when eruption frequency is also considered. Aira shows the largest increase in ranking, rising from 49th based on median unweighted FDS to 2nd based on its AADS, while Abu had the largest decrease, falling from 8th to 59th. Only one volcano, Yonemaru-Sumiyoshiike, maintained the same ranking under both metrics (38th). Volcanoes such as Fujisan remain highly ranked across both metrics as they combine high disruption potential with moderate eruption frequencies, whereas other volcanoes rise or fall substantially depending on whether rare extreme events or annual expected disruption is emphasised.

https://doi.org/10.5194/egusphere-2026-5468
Preprint. Discussion started: 11 September 2026
© Author(s) 2026. CC BY 4.0 License.

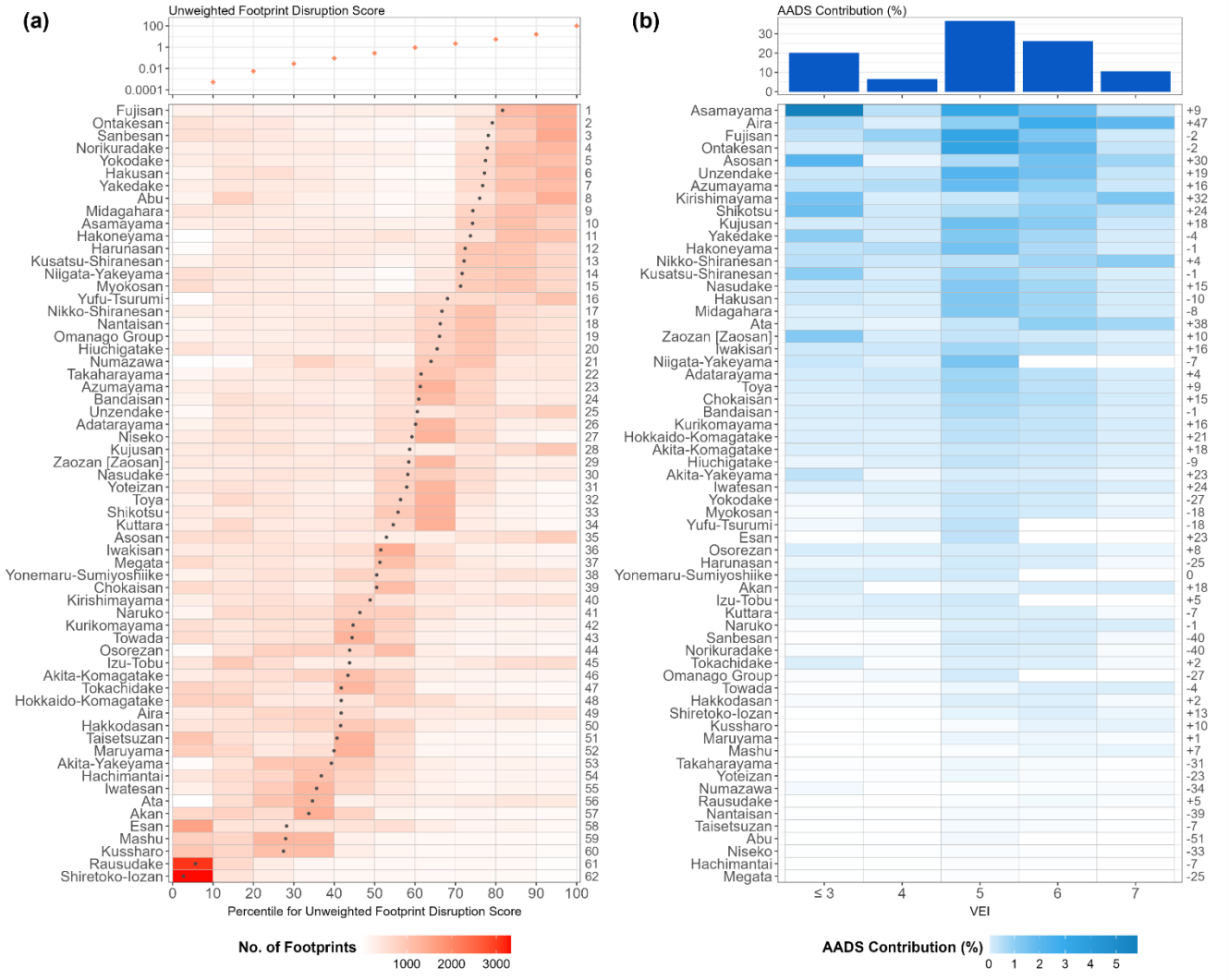

Figure 8: Heatmap of (a) unweighted footprint disruption scores (FDS) and (b) average annual disruption score (AADS) for each volcano. (a) Volcanoes are ranked (number on the right) by the percentile of their median FDS, indicated by the black dots on the heatmap. The points above the heatmap show the absolute values corresponding to the percentile bin thresholds, calculated from all simulated tephra fall footprints. (b) Volcanoes are ranked by their contribution to the annual expected electricity disruption for mainland Japan, expressed as a percentage. The bar plot above the heatmap shows the total contribution of each VEI class. Numbers on the right indicate the change in ranking relative to (a), where positive values denote that a volcano moved up in rank.

3.3 Spatial distribution of average annual disruption scores (AADS)

3.3.1 Disruption hotspots

The spatial distribution of average annual disruption scores (AADS) reveals a strong concentration of high disruption potential within the major metropolitan regions of mainland Japan (Fig. 9). The largest contributions to annual expected electricity disruption occur in the Tokyo, Osaka, and Nagoya metropolitan areas, where high criticality infrastructure coincide with large

https://doi.org/10.5194/egusphere-2026-5468
Preprint. Discussion started: 11 September 2026
© Author(s) 2026. CC BY 4.0 License.

populations. Hotspot analysis identifies statistically significant clusters of elevated AADS not only in these major urban centres but also in several smaller cities such as Anan and Hitachinaka (Fig. 9b). These locations contain infrastructure assets that contribute disproportionately to annual expected disruption despite being outside the largest population centres

The exceedance-based maps show that disruption potential remains concentrated in central Japan across a wide range of annual exceedance rates (Fig. 9c–h). At high exceedance rates of 0.02, only a limited number of grid cells exhibit non-zero disruption scores, with the largest values concentrated in central Japan. As exceedance rates decrease and rarer disruption scenarios are considered, affected areas expand to include much of northern Japan but the highest disruption scores are still concentrated in central Japan throughout the exceedance spectrum. At relatively low exceedance rates of 0.001 (Fig. 9g), almost all grid cells affected by tephra fall have non-zero disruption scores. A consistent spatial contrast is evident between the Pacific and Sea of Japan coasts. At a given exceedance rate, grid cells along the Pacific coast generally exhibit larger disruption scores than those along the Sea of Japan, reflecting the combined influence of higher infrastructure criticality and predominantly westerly winds resulting in greater exposure to tephra fall footprints from multiple volcanoes (Fig. 9c-h).

https://doi.org/10.5194/egusphere-2026-5468
Preprint. Discussion started: 11 September 2026
© Author(s) 2026. CC BY 4.0 License.

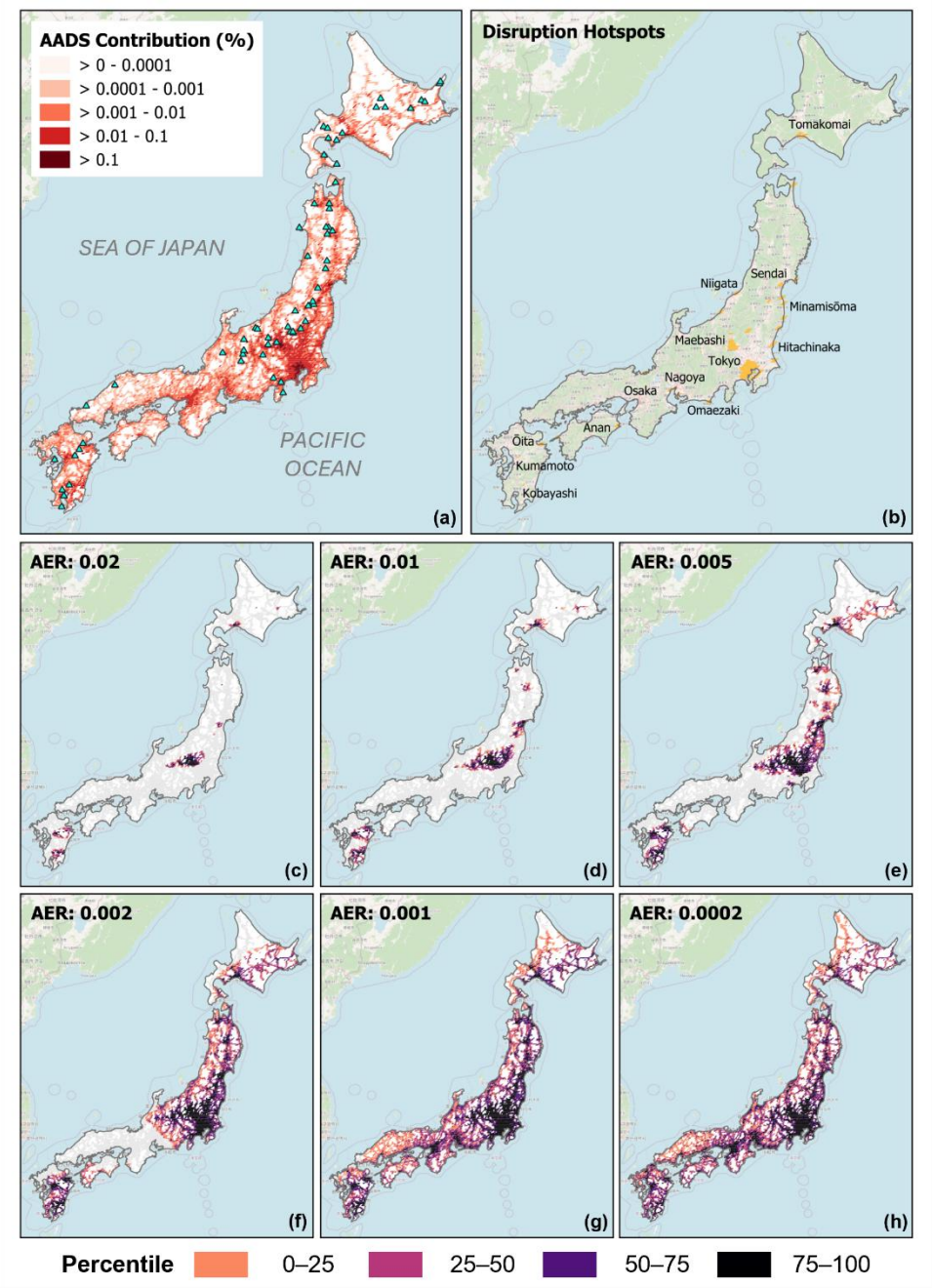

Figure 9: (a) Average annual disruption score (AADS) of each 5 x 5 km grid cell, expressed as a percentage contribution to the overall AADS for mainland Japan. The blue triangles represent the 62 study volcanoes on mainland Japan. Hotspot analysis was conducted on the gridded AADS using the Getis-Ord Gi* statistic to identify (b) disruption hotspots (90 % confidence). Cities containing disruption hotspots are labelled. Grid cells with non-zero disruption scores at specific annual exceedance rates (AERs) – (c) 0.02, (d) 0.01, (e) 0.005, (f) 0.002, (g) 0.001 and (h) 0.0002 – are coloured by the percentile bin of their disruption score equalled or exceeded, calculated from all non-zero cells for the given AER. Cells that are disrupted (regardless of AER) are shown in grey. Base map: © OpenStreetMap contributors

https://doi.org/10.5194/egusphere-2026-5468
Preprint. Discussion started: 11 September 2026
© Author(s) 2026. CC BY 4.0 License.

3.3.2 Average annual disruption score (AADS) by prefecture

Aggregating average annual disruption scores (AADS) by prefecture highlights substantial regional variation in disruption potential across mainland Japan (Fig. 10). Prefectures in central and northern Japan have the largest AADS and contribute most to the annual expected electricity disruption for mainland Japan (Fig. 10a). Normalising AADS by prefecture area highlights differences between concentrated and dispersed disruption potential. For example, Hokkaido ranks fifth by prefecture contribution to the total AADS for mainland Japan, but its ranking decreases substantially when AADS is expressed per unit area because disruption potential is spread across a much larger geographic region. By contrast, prefectures within the Tokyo Metropolitan Area retain high rankings under both metrics, reflecting a concentration of high criticality infrastructure and population within a relatively small area (Fig. 10b). The prefecture-scale analysis reinforces the prominence of central Japan as the region with the highest disruption potential.

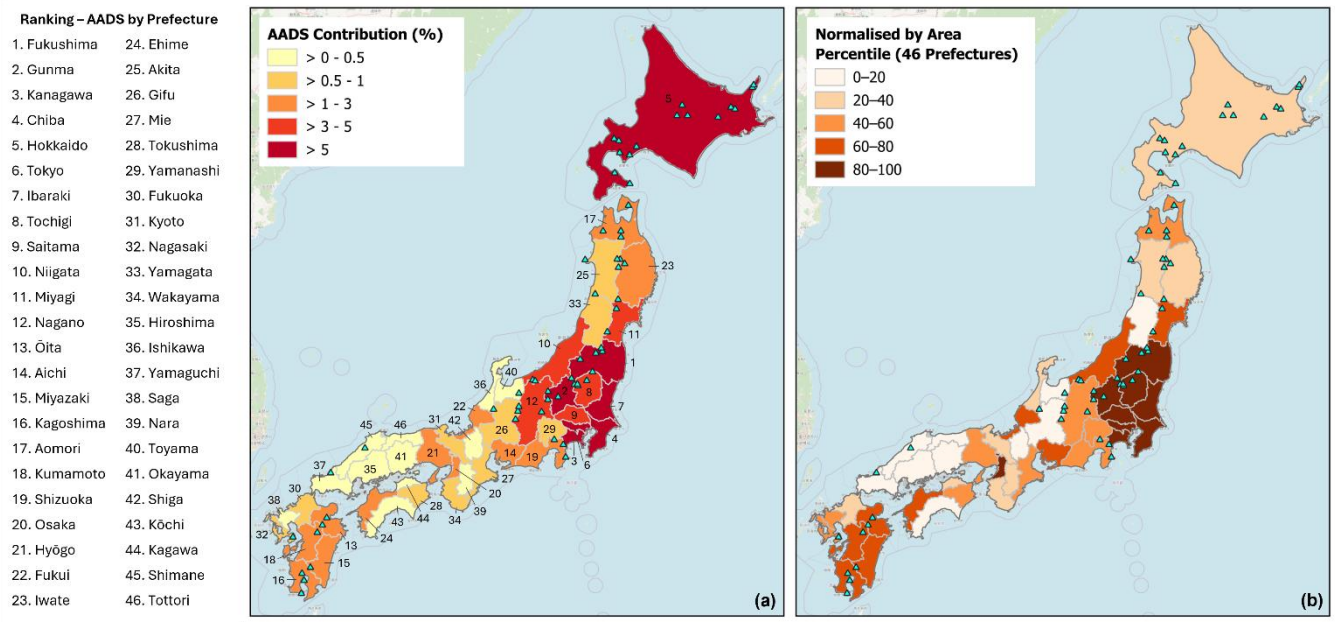

Figure 10: Annual average disruption score (AADS) by prefecture, expressed as the (a) percentage contribution to the total AADS for mainland Japan. Prefectures are labelled by the ranking of their AADS. The AADS for each prefecture is also (b) normalised by the prefecture area and classified into percentile bins. Volcanoes considered in this study are represented by the blue triangles. Base map: © OpenStreetMap contributors

3.4 Footprint disruption scores (FDS) of historical eruptions

3.4.1 Kirishimayama: Shinmoedake eruption in 2011

The 2011 VEI 3 Shinmoedake eruption provides a useful benchmark for interpreting the simulated disruption scores because its impacts on electricity infrastructure are well documented (Magill et al., 2013; Nakada et al., 2013; Maeno et al., 2014). The main urban areas affected by tephra fall reported by Magill et al. (2013) were Miyakonojo City (~27 km SE), Takaharu Town

https://doi.org/10.5194/egusphere-2026-5468
Preprint. Discussion started: 11 September 2026
© Author(s) 2026. CC BY 4.0 License.

centre (12 km E), Mimata Town centre (30 km SE) and Nicihinan City centre (58 km SE). Magill et al. (2013) estimated electricity infrastructure assets affected by tephra fall (tephra load > 0 to 30 kg/m^2) to include four hydroelectric power stations, approximately 260 km of transmission lines, as well as 16 substations within the Kyushu Electric Power Company (KEPC) network. Although incidents of electricity leakage (partial discharge: n=54) and insulator flashover (n=29) were reported, widespread electricity supply disruptions were largely avoided through a combination of resilient insulator design, removal of tephra by wind and rain, and cleaning operations by KEPC (Magill et al., 2013).

The estimated footprint disruption score (FDS) for the event falls between the 84th and 93rd percentile of simulated VEI ≤ 3 eruptions from Kirishimayama (Fig. 11), indicating that the event was more disruptive than most small intensity eruptions. This relatively high value reflects the southeastwards dispersal of tephra towards populated areas and electricity infrastructure. By comparison, the simulated eruption with the smallest non-zero FDS deposits tephra predominantly northwest of the volcano, where infrastructure exposure is limited, whereas the most disruptive simulated scenario disperses tephra northeastwards towards Miyazaki City and other areas containing more electricity infrastructure. These results highlight that wind-driven differences in tephra dispersal can produce substantial variation in disruption potential, even for eruptions of similar intensity from the same volcano.

https://doi.org/10.5194/egusphere-2026-5468
Preprint. Discussion started: 11 September 2026
© Author(s) 2026. CC BY 4.0 License.

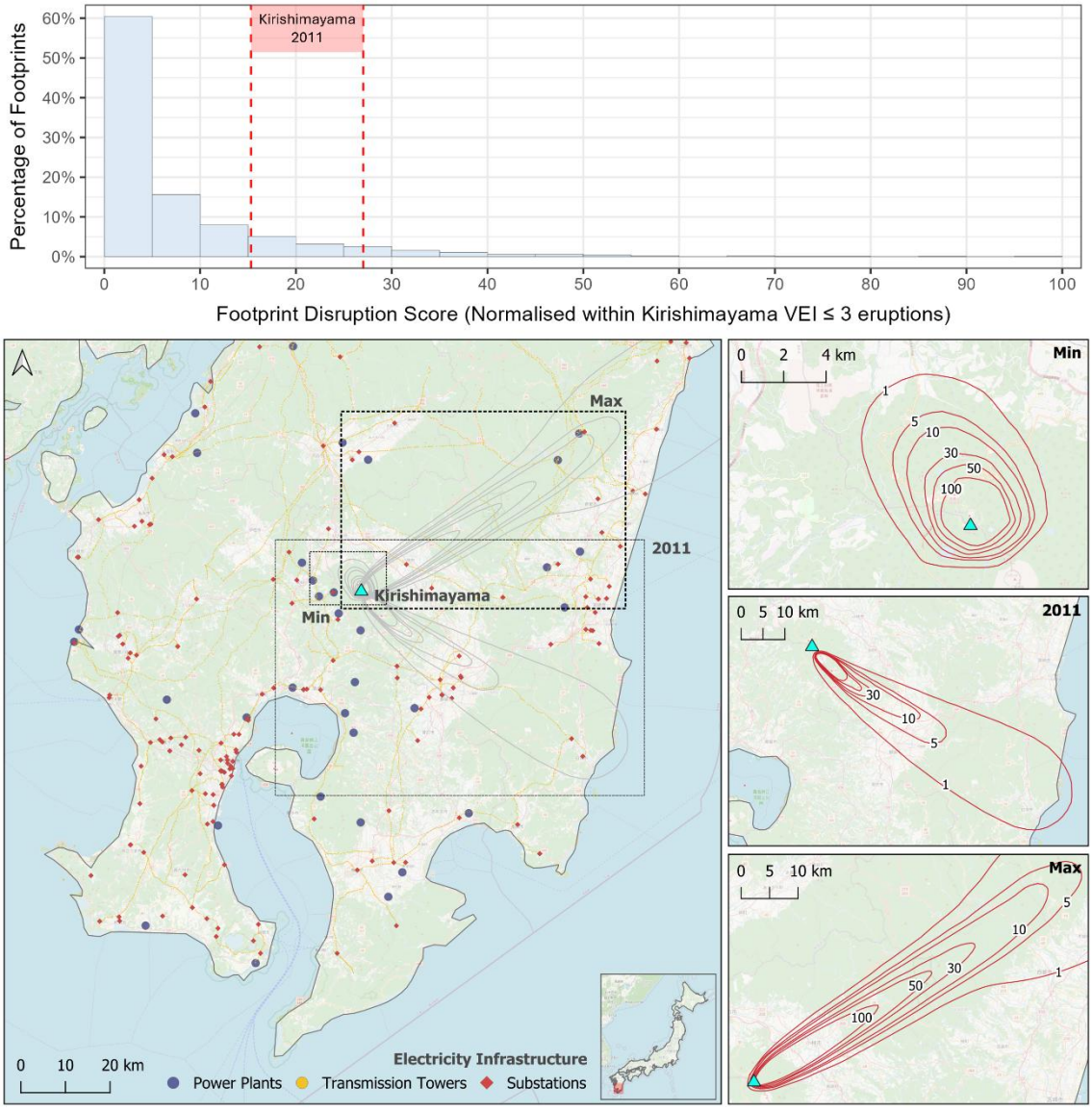

Figure 11: Footprint disruption scores (FDS) for the 2011 Shinmoedake eruption at Kirishimayama compared with simulated VEI ≤ 3 eruptions from the volcano (histogram). The maps show the electricity infrastructure together with the tephra isopaches for the 2011 event (from Magill et al., 2013) and the simulated eruptions with the minimum non-zero FDS and maximum FDS. For all isopach maps, the thickness corresponding to 1, 5, 10, 30, 50 and 100 mm are shown. Base map: © OpenStreetMap contributors

3.4.2 Fujisan: Hoei eruption in 1707

A Hoei-like eruption of Fujisan has been used as a reference eruption scenario to develop countermeasures against widespread tephra fall in Tokyo and surrounding prefectures (Central Disaster Prevention Council, 2020). Historical accounts indicate severe damage in proximal downwind areas, and respiratory problems were reported for residents in the area that is now Tokyo (Miyaji et al., 2011). A comparable eruption today is expected to pose a significant threat to electricity service delivery in

https://doi.org/10.5194/egusphere-2026-5468
Preprint. Discussion started: 11 September 2026
© Author(s) 2026. CC BY 4.0 License.

Tokyo, particularly as the Tokyo Bay area has many thermal power plants with air filtration systems that may become clogged or partially blocked with tephra (Yamamoto and Nakada, 2015). Disruption scores calculated from the cumulative Hoei tephra fall deposit lie between the 56th and 81st percentile of simulated VEI 5 eruptions from Fujisan (Fig. 12). This indicates that, although the Hoei eruption would represent a substantial disruption scenario if repeated today, it does not correspond to the most disruptive outcomes generated by the simulations. The least disruptive simulated scenario deposits tephra predominantly offshore to the southeast, limiting exposure of critical infrastructure. The most disruptive scenarios deposit tephra eastwards, corresponding with the predominant wind direction for the area, over a larger area of the Tokyo Metropolitan Area where high criticality electricity infrastructure and large populations are concentrated.

https://doi.org/10.5194/egusphere-2026-5468
Preprint. Discussion started: 11 September 2026
© Author(s) 2026. CC BY 4.0 License.

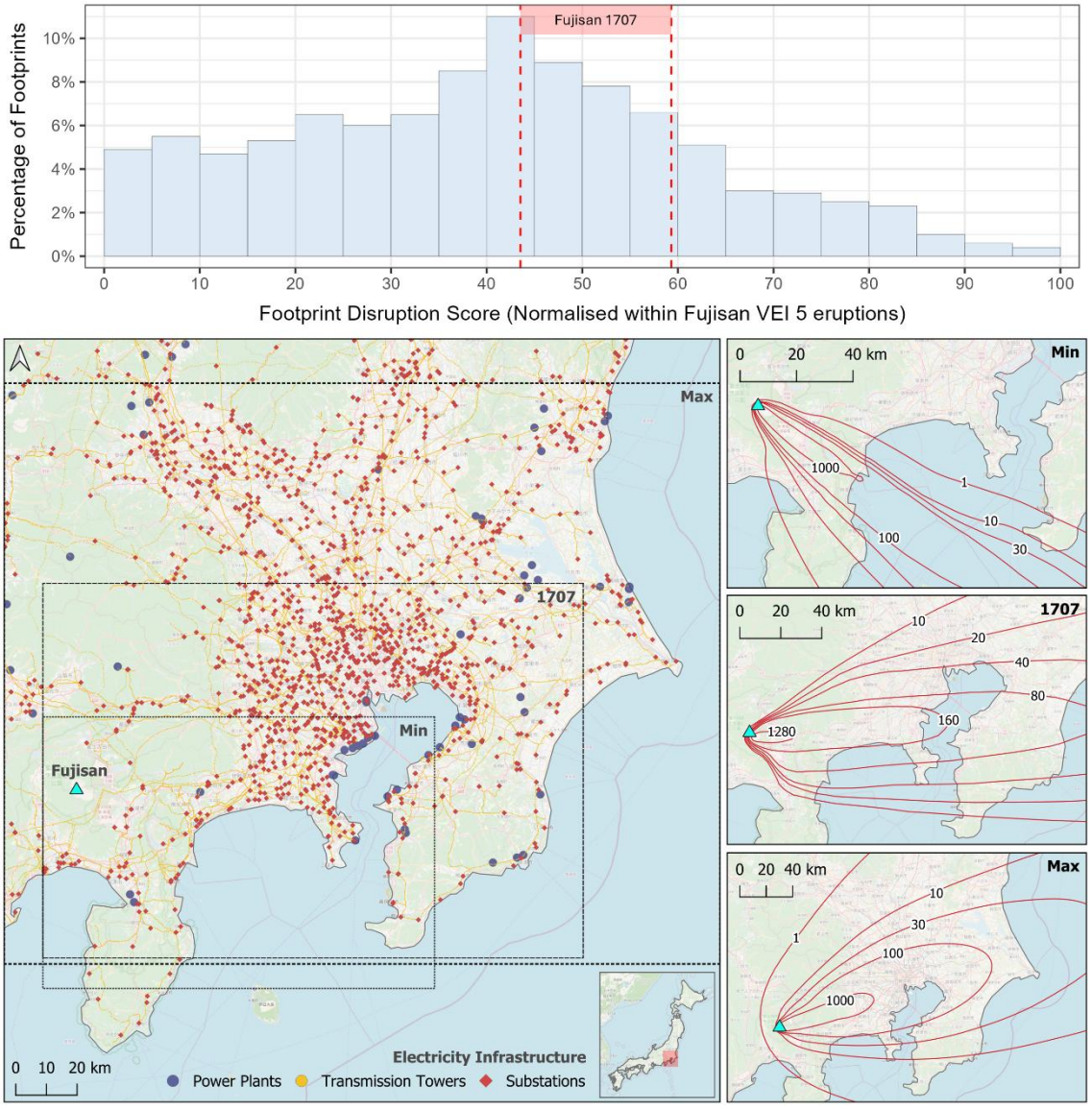

Figure 12: Footprint disruption scores (FDS) for the 1707 Hoei eruption of Fujisan compared with simulated VEI 5 eruptions for Fujisan (histogram). The maps show the electricity infrastructure together with the tephra isopaches for the Hoei eruption (from Miyaji et al., 2011) and the simulated eruptions with the minimum non-zero FDS and maximum FDS. The Hoei eruption isopaches correspond to tephra thicknesses of 10, 20, 40, 80, 160 and 1280 mm, while the simulated eruption isopaches correspond to thicknesses of 1, 10, 30, 100 and 1000 mm. Base map: © OpenStreetMap contributors

https://doi.org/10.5194/egusphere-2026-5468
Preprint. Discussion started: 11 September 2026
© Author(s) 2026. CC BY 4.0 License.

4 Discussion

4.1 Contributors to disruption potential

The positively skewed distribution of footprint disruption scores (FDS) indicates that relatively severe disruptions to mainland Japan's electricity network are possible but relatively uncommon. Two factors appear to drive this pattern. Firstly, Japan's geography, being a long, narrow archipelago approximately 300 km wide, limits the exposure of electricity infrastructure to many of the large tephra fall events. Although intense explosive eruptions can deposit tephra over distances approaching 1,000 km (Biass et al., 2023), the predominantly east blowing winds typically transport a proportion of tephra offshore over the Pacific Ocean, reducing exposure of critical infrastructure on the mainland. Second, disruption potential depends not only on hazard intensity and distribution but also on the criticality of the exposed assets (Hayes et al., 2022a; Thacker et al., 2017). Outside the major urban centres, electricity infrastructure criticality is relatively distributed across mainland Japan (Fig. 4), reducing the likelihood that impacts to individual assets will produce widespread electricity disruption. This pattern is consistent with the increasing diversification and decentralisation of Japan's energy system following the 2011 Fukushima disaster (Ogimoto et al., 2013; Wagner et al., 2021), reducing reliance on a small number of highly critical assets. The largest disruption scores occur only when extensive tephra fall footprints coincide with highly critical infrastructure. These scenarios represent the upper tail of the disruption distribution and are therefore particularly important for resilience planning. However, there are large uncertainties associated with these scenarios as high intensity eruptions are infrequent; thus, there is limited information to constrain eruption parameters and calculate eruption probabilities (Hayes et al., 2022b) for risk assessments.

The volcano rankings illustrate how disruption potential emerges from the interaction between hazard characteristics and infrastructure criticality. Volcanoes with the highest median unweighted FDS – Fujisan, Ontakesan, and Sanbesan (last known eruptions: 1708, 2014 and 650 CE, respectively) – reach those rankings for different reasons. Fujisan is located approximately 100 km southwest of the Tokyo Metropolitan Area, where the concentration of high criticality electricity infrastructure means that relatively moderate shifts in tephra dispersal can substantially increase disruption severity. Ontakesan and neighbouring volcanoes such as Norikuradake and Yakedake demonstrate a different mechanism, with high rankings driven by concentrations of electricity generation assets rather than proximity to the largest population centres. By comparison, Sanbesan is situated within a region of relatively low infrastructure criticality but has the largest proportion of footprints (30 %) within the highest FDS decile as it can potentially produce very disruptive eastward dispersal scenarios capable of simultaneously affecting the Tokyo, Osaka and Nagoya metropolitan areas. Although Sanbesan has not erupted since 650 CE, geological evidence indicates an eruption record containing multiple VEI 6 events (Matsui and Inoue, 1971; Fukuoka and Matsui, 2002; Albert et al., 2018; Auer et al., 2022) and tephra from the volcano has been found across the Kansai and Chugoku regions (Maruyama et al., 2020), suggesting that widespread disruption from future large eruptions is plausible.

https://doi.org/10.5194/egusphere-2026-5468
Preprint. Discussion started: 11 September 2026
© Author(s) 2026. CC BY 4.0 License.

Incorporating eruption frequency substantially alters the prioritisation of volcanoes. Whereas Fujisan ranks highest when considering disruption severity alone, Asamayama becomes the largest contributor to annual expected disruption because of its high eruption frequency and its relatively high disruption potential. Asamayama is one of the most active volcanoes in Japan and poses tephra fall risk to the Tokyo Metropolitan Area due to its frequent VEI 2 eruptions that occur on a decadal scale (Suzuki, 2018). Tephra from small eruptions (VEI 1–2) have reached Tokyo multiple times, including in 2004 and 2009 (Nakada and Takeo, 2013), with larger eruptions such as the 1783 (VEI 4) event depositing tephra in the Kanto (containing Tokyo) and Tohoku regions (Suzuki, 2018). Similarly, Aira rises dramatically in the rankings because it combines comparatively frequent large eruptions with the potential to affect highly critical infrastructure. Conversely, volcanoes such as Sanbesan decline in rank because their long recurrence intervals reduce their overall contribution to annual expected disruption despite their capacity to generate highly disruptive scenarios. These results demonstrate that disruption severity and disruption risk are distinct concepts. Identifying volcanoes capable of producing extreme disruptions is important for contingency planning, but prioritising long-term risk reduction also requires consideration of eruption frequency.

Temporal factors may further modify disruption potential. Although seasonal wind conditions affect the direction and distance of tephra dispersal, which alters the electricity infrastructure assets exposed, seasonal variations are relatively modest. The slightly greater variability observed during summer for unweighted FDS suggests more variable atmospheric conditions, coinciding with Japan's typhoon season, which increases the range of possible disruption outcomes. Seasonal weather conditions may also influence infrastructure vulnerability. For example, wet tephra is more conductive than dry tephra and can increase the likelihood of insulator flashover and electrical disruption (Homma et al., 2019). Wet tephra also produces a greater load, which can increase the probability of structural damage (Wardman et al., 2012). However, wet conditions do not necessarily exacerbate disruption, as observed during the 2011 Shinmoedake eruption, where most electricity disruption incidents occurred during a period of light rainfall and largely resolved after subsequent heavy rainfall removed deposited tephra from electricity infrastructure (Magill et al., 2013). Temporal variations in electricity demand provide an additional consideration. Although disruption potential remains broadly similar throughout the year, equivalent disruption events occurring during winter or summer demand peaks would likely have greater operational consequences for electricity supply.

4.2 Spatial distribution of disruption potential

The spatial distribution of disruption potential reflects the interaction between the spatial distribution of hazard intensity and frequency from multiple source volcanoes, and the spatial distribution of asset vulnerability and criticality. Areas with the highest disruption potential are not necessarily those closest to volcanoes, but those where frequent or intense tephra fall coincides with highly critical assets. This is particularly evident along the Pacific coast, where many major urban centres are located downwind of multiple active volcanoes under the prevailing east blowing winds. Previous national-scale tephra fall assessments have similarly identified eastern and northeastern Japan as experiencing the highest frequencies of tephra fall (Uesawa et al., 2022). Many of the disruption hotspots identified in this study, including the Tokyo, Sendai, and Maebashi

https://doi.org/10.5194/egusphere-2026-5468
Preprint. Discussion started: 11 September 2026
© Author(s) 2026. CC BY 4.0 License.

regions, occur within these areas of elevated hazard. This highlights that the highest disruption potential arises when high tephra hazard coincides with concentrated electricity demand and critical infrastructure. These areas may therefore benefit most from more detailed risk assessments and targeted mitigation measures to enhance the resilience of the electricity network to tephra fall.

The hotspot analysis also reveals the importance of considering infrastructure function in addition to population exposure. While many hotspots correspond to major metropolitan areas, several others are associated with electricity generation facilities, including those near Tomakomai, Minamisoma and Hitachinaka. These locations emerge because power generation assets generally have higher criticality than other electricity asset types, considering that the loss of a single facility can affect electricity supply over a wide geographic area. As a result, areas containing major generation facilities can contribute substantially to disruption potential even where local population densities are comparatively low. The importance of generation infrastructure in raising the potential of disruption in our study is consistent with observations from other hazard events in Japan. Following the 2011 Tohoku earthquake, approximately 8 % of Japan's generation capacity was lost, resulting in power outages affecting 5.27 million households and rolling blackouts across the Tokyo Metropolitan Area (Nakano, 2011). Similarly, the 2022 Fukushima earthquake caused the shutdown of several thermal power plants, leading to electricity outages affecting approximately 2.1 million households in the Tokyo Metropolitan Area (Tokyo Electric Power Company Holdings, 2022). Although historical electricity disruptions from volcanic eruptions in Japan have generally been more localised, these earthquake events demonstrate how impacts to major generation facilities can propagate through the electricity network, suggesting that impactful tephra falls affecting major power plants could similarly result in widespread electricity disruption.

4.3 Limitations and future work

The disruption scoring framework was developed as a national-scale screening tool and therefore required balancing model complexity, data availability, and computational efficiency. A key simplification was the repositioning of tephra fall simulations generated for Fujisan to represent all volcanoes. This approach implicitly assumes broadly similar eruption source characteristics and wind conditions across mainland Japan. While this simplification does not capture volcano-specific eruptive behaviour or local atmospheric conditions, it enables consistent comparison of disruption potential at the national scale across a large number of volcanoes. Lower-voltage distribution assets such as local poles and lines were also not considered, therefore more localised disruptions associated with smaller tephra fall footprints may not be fully captured in this study. Consequently, the tool provides a first-order representation of disruption potential from select key infrastructure rather than a replacement for detailed site-specific risk assessments.

A second limitation concerns the representation of an 'eruption'. Each simulated tephra fall footprint was produced by a single explosive phase from a volcano, whereas in reality, eruptions can comprise multiple phases that may continue intermittently for anywhere from days to decades (Jenkins et al., 2007; Bebbington and Jenkins, 2019). For example, the 1707 Hoei eruption

https://doi.org/10.5194/egusphere-2026-5468
Preprint. Discussion started: 11 September 2026
© Author(s) 2026. CC BY 4.0 License.

lasted 16 days, with some quiet periods within the sequence (Miyaji et al., 2011). In practice, the time available between explosive eruptive phases may allow deposited tephra to be removed from infrastructure, reducing the impacts of subsequent tephra falls. Thus, our results should be interpreted as the unmitigated disruption from one explosive phase, which is important for understanding where potential mitigation activities might be most beneficial to minimise disruptions.

The framework also adopts a simplified representation of infrastructure vulnerability. Generic fragility functions per electricity asset type and common consequence weights were applied across mainland Japan. Spatial variations in infrastructure vulnerability arising from differences in tephra properties, infrastructure design, and local mitigation measures were not considered. Whilst tephra thickness is often correlated with impact severity, other properties such as grain size, composition, and electrical conductivity can also influence infrastructure performance (G. Wilson et al., 2014; G. Wilson et al., 2017; Homma et al., 2019). For example, the 2016 eruption of Asosan caused relatively large electricity disruption despite modest tephra fall as the presence of a highly acidic lake prior to the eruption produced fine-grained and highly conductive tephra, which enhanced the potential for flashover, resulting in a power outage to approximately 29,000 houses (Nagai and Nakada, 2022). Operational and mitigation measures implemented at local scales also influence tephra fall impacts and disruption severity. Covered substations near Kagoshima, for example, have been designed to accommodate the frequent tephra falls from Sakurajima (Aira) volcano, reducing the likelihood of flashover and operational disruption (Durand, 2001; Wardman et al., 2012). The level of disruption also depends on system resilience, as demonstrated during the 2011 Shinmoedake eruption when network rerouting allowed for cleanup of transformers to be conducted without electricity supply disruptions (Magill et al., 2013). Such factors are better addressed through detailed volcano- or site-specific studies that build upon the screening approach developed here.

Future studies could focus on areas and volcanoes identified as having particularly high disruption potential, including the Tokyo Metropolitan Area and volcanoes such as Fujisan, Asamayama, and Ontakesan. Such studies could incorporate locally specific vulnerability information (e.g. maximum tephra accumulation on insulators; Homma et al., 2024), infrastructure operating characteristics, and mitigation measures. The representation of the electricity network can also be improved by incorporating more detailed attributes into existing exposure datasets, such as whether an asset is over or underground, and by developing datasets with greater completeness and coverage. Additionally, the current framework considers tephra fall alone, whereas volcanic eruptions frequently generate multiple hazards capable of affecting infrastructure systems. For example, lahars may affect hydroelectric facilities through sediment deposition in reservoirs and waterways (Wilson et al., 2014). Extending the framework to incorporate multiple volcanic hazards would provide a more comprehensive assessment of critical infrastructure disruption risk.

https://doi.org/10.5194/egusphere-2026-5468
Preprint. Discussion started: 11 September 2026
© Author(s) 2026. CC BY 4.0 License.

5 Conclusion

We developed a probabilistic disruption scoring framework for distributed critical infrastructure systems to quantify the relative disruption potential of different hazard sources and spatial areas. By integrating hazard intensity, occurrence probability, infrastructure vulnerability, and asset criticality into a common disruption metric, the framework provides a systematic approach for identifying the hazard sources and locations most likely to contribute to infrastructure disruption. Application of the framework to tephra fall impacts on Japan's electricity network demonstrates three key findings. First, disruption potential is strongly controlled by the spatial coincidence of tephra fall hazard and highly critical infrastructure. Second, volcano rankings depend substantially on whether disruption severity alone or disruption severity and eruption frequency is considered. Fujisan produces the most severe electricity disruption scenarios conditional on an eruption, whereas Asamayama is the largest contributor to annual expected disruption once eruption frequency is incorporated. Third, disruption hotspots are concentrated in major metropolitan areas, particularly the Tokyo, Osaka, and Nagoya regions, as well as in areas containing critical electricity generation facilities. These results provide a quantitative basis for prioritising volcanic risk reduction and infrastructure resilience measures. More broadly, they demonstrate the importance of considering both disruption severity and event frequency when evaluating hazard sources and identifying priorities for risk management.

Although demonstrated here for tephra fall impacts on electricity infrastructure in Japan, the framework can be readily transferred to other regions, infrastructure sectors, and natural hazards. As it relies on widely available datasets and scalable analytical methods, it can be used as a first-order screening tool to identify priority hazard sources, locations, and infrastructure assets for more detailed risk and resilience assessments. Such assessments are particularly valuable in regions where numerous hazard sources interact with spatially extensive and interconnected critical infrastructure systems, providing a systematic and quantitative evidence base for the prioritisation of limited risk reduction resources.

Code and data availability

The code and datasets used are accessible via:

1. TephraProb package (Biass et al., 2016) – https://github.com/e5k/TephraProb
2. Global Power Plant Database (Byers et al., 2021) – https://datasets.wri.org/datasets/global-power-plant-database
3. OpenStreetMap data (OpenStreetMap Contributors, 2025) – QuickOSM plugin in QGIS
4. WorldPop Population Counts (Bondarenko et al., 2025) – https://hub.worldpop.org/geodata/summary?id=73950
5. Electricity demand (OCCTO, 2025) – https://www.occto.or.jp/houkokusho/2025/2025_nenjihoukokusho.html
6. Holocene Volcano List (GVP, 2025) – https://volcano.si.edu/volcanolist_holocene.cfm
7. Confirmed Holocene Eruptions (GVP, 2025) – https://volcano.si.edu/search_eruption.cfm
8. European Centre for Medium Range Weather Forecasts (ECMWF) ERA5 (Hersbach et al., 2023) – Climate Data Store (CDS) Application Program Interface (API)

https://doi.org/10.5194/egusphere-2026-5468
Preprint. Discussion started: 11 September 2026
© Author(s) 2026. CC BY 4.0 License.

The code developed in this study is available at https://github.com/vharg/CI-Disruption-JP.

Supplement link

The link to the supplement will be included by Copernicus, if applicable.

Supplementary Material A: Probabilistic Tephra Fall Modelling Approach

Supplementary Material B: Eruption Frequency-Magnitude Relationships

Author contributions

The project was conceptualized by RXNT, JLH, SFJ and MJ. RXNT, JLH and SFJ developed the methodology with support from DL, MJ, EF, JW, YM and TK. RXNT and JLH developed the code and performed the simulations. The original draft was written by RXNT and JLH. All authors contributed to reviewing and editing the manuscript.

Competing interests

The authors declare that they have no conflict of interest.

Disclaimer

Copernicus Publications adds a standard disclaimer: "Copernicus Publications remains neutral with regard to jurisdictional claims made in the text, published maps, institutional affiliations, or any other geographical representation in this paper. While Copernicus Publications makes every effort to include appropriate place names, the final responsibility lies with the authors. Views expressed in the text are those of the authors and do not necessarily reflect the views of the publisher."

Acknowledgements

We thank Professor Setsuya Nakada for discussions during the early stages of the project.

Financial support

RXNT, JLH, SFJ, and MJ acknowledge funding from the AXA Joint Research Initiative (Volcanic Risk in Asia). RXNT, SFJ and DL acknowledge the Ministry of Education, Singapore, under its MOE Academic Research Fund Tier 3 InVEST project (Award MOE-MOET32021-0002) for funding support. JLH acknowledges funding from the New Zealand Ministry of

© Author(s) 2026. CC BY 4.0 License.

Business, Innovation and Employment (MBIE) through the Strategic Science Investment Fund Infrastructure and Systems Vulnerability project.

Review statement

The review statement will be added by Copernicus Publications listing the handling editor as well as all contributing referees according to their status anonymous or identified.

References

Alberico, I., Petrosino, P., and Lirer, L.: Volcanic hazard and risk assessment in a multi-source volcanic area: The example of Napoli city (Southern Italy), Natural Hazards and Earth System Sciences, 11, 1057–1070, https://doi.org/10.5194/nhess-11-1057-2011, 2011.

Albert, P. G., Smith, V. C., Suzuki, T., Tomlinson, E. L., Nakagawa, T., McLean, D., Yamada, M., Staff, R. A., Schlolaut, G., Takemura, K., Nagahashi, Y., and Kimura, J.-I.: Constraints on the frequency and dispersal of explosive eruptions at Sambe and Daisen volcanoes (South-West Japan Arc) from the distal Lake Suigetsu record (SG06 core), Earth-Science Reviews, 185, 1004–1028, https://doi.org/10.1016/j.earscirev.2018.07.003, 2018.

Auer, A., Kamei, A., and Endo, D.: Sanbe volcano: Long-term evolution of an arc magmatic system, Island Arc, 31, https://doi.org/10.1111/iar.12453, 2022.

Bebbington, M. S., and Jenkins, S. F.: Intra-eruption forecasting. Bulletin of Volcanology, 81, 34, https://doi.org/10.1007/s00445-019-1294-9, 2019.

Biass, S., Scaini, C., Bonadonna, C., Folch, A., Smith, K., and Höskuldsson, A.: A multi-scale risk assessment for tephra fallout and airborne concentration from multiple Icelandic volcanoes – Part 1: Hazard assessment, Natural Hazards and Earth System Sciences, 14, 2265–2287, https://doi.org/10.5194/nhess-14-2265-2014, 2014.

Biass, S., Bonadonna, C., Connor, L., and Connor, C.: TephraProb: A Matlab package for probabilistic hazard assessments of tephra fallout, Journal of Applied Volcanology, 5, 10, https://doi.org/10.1186/s13617-016-0050-5, 2016.

Biass, S., Jenkins, S. F., Hayes, J. L., Williams, G. T., Meredith, E. S., Tennant, E., Yang, Q., Lerner, G. A., Burgos, V., Syarifuddin, M., and Verolino, A.: How well do concentric radii approximate population exposure to volcanic hazards?, Bull Volcanol, 86, 3, https://doi.org/10.1007/s00445-023-01686-5, 2023.

Bonadonna, C.: Probabilistic modeling of tephra dispersal: Hazard assessment of a multiphase rhyolitic eruption at Tarawera, New Zealand, Journal of Geophysical Research, 110, B03203, https://doi.org/10.1029/2003JB002896, 2005.

Bondarenko, M., Priyatikanto, R., Tejedor-Garavito, N., Zhang, W., McKeen, T., Cunningham, A., Woods, T., Hilton, J., Cihan, D., Nosatiuk, B., Brinkhoff, T., Tatem, A., and Sorichetta, A.: Constrained estimates of 2015-2030 total number of

https://doi.org/10.5194/egusphere-2026-5468
Preprint. Discussion started: 11 September 2026
© Author(s) 2026. CC BY 4.0 License.

people per grid square at a resolution of 3 arc (approximately 100m at the equator) (R2025A version v1), WorldPop - School of Geography and Environmental Science, University of Southampton [data set], DOI:10.5258/SOTON/WP00839, 2025.

Bruneau, M., Chang, S.E., Eguchi, R.T., Lee, G.C., O'Rourke, T.D., Reinhorn, A.M., Shinozuka, M., Tierney, K., Wallace, W.A. and von Winterfeldt, D.: A Framework to Quantitatively Assess and Enhance the Seismic Resilience of Communities, Earthquake Spectra, 19(4), 733-752, https://doi.org/10.1193/1.1623497, 2003.

Byers, L., Friedrich, J., Hennig, R., Kressig, A., Li, X., Valeri, L. M., and McCormick, C.: Global Power Plant Database (1.3.0), World Resources Institute [data set], https://datasets.wri.org/datasets/global-power-plant-database, 2021.

Central Disaster Prevention Council.: Wide-area Ashfall Countermeasures in the Event of a Large-Scale Eruption – Impacts of Ashfall and Countermeasures in the Tokyo Metropolitan Area – Using the Eruption of Mt. Fuji as a Model Case, Cabinet Office, Government of Japan, https://www.bousai.go.jp/kazan/kouikikouhaiworking/pdf/syutohonbun.pdf, 2020.

Cha Y., White, C. J., Gonzalez, P. L. M., Wallace, E., Harkin, D., Brett, L., Mattu, K., Smith, R. S., Thom, C., Alix, M. D., Olbert, C., Burnett, L., Hampton, E., Sheppard, A., Campbell, A., Rees, G., and Steller, R.: Assessing the cascading impacts of natural hazards on Critical National Infrastructure (CNI) using Scotland as a case study, npj Nat. Hazards, 2, 108, https://doi.org/10.1038/s44304-025-00161-9, 2025.

Dilley, M., Chen, R. S., Deichmann, U. K., Lerner-Lam, A. L., and Arnold, M.: Natural Disaster Hotspots: A Global Risk Analysis, World Bank Group, Washington, D.C, http://documents.worldbank.org/curated/en/621711468175150317, 2005.

Durand, M.: Impacts of, and responses to ashfall in Kagoshima from Sakurajima Volcano: Lessons for New Zealand, Institute of Geological & Nuclear Sciences Limited, 2001.

Eidsvig, U. M. K., Kristensen, K., and Vangelsten, B. V.: Assessing the risk posed by natural hazards to infrastructures, Nat. Hazards Earth Syst. Sci., 17, 481–504, https://doi.org/10.5194/nhess-17-481-2017, 2017.

Fischhoff, B., and Morgan, M. G.: The science and practice of risk ranking, in: Risk analysis and human behavior, Routledge, 379–389, https://doi.org/10.4324/9780203140710, 2013.

Fujita, E., Ueda, H., and Nakada, S.: A New Japan Volcanological Database, Frontiers in Earth Science, 8, 205, https://doi.org/10.3389/feart.2020.00205, 2020.

Fukuoka, T., and Matsui, S.: Stratigraphy of pyroclastic deposits post-dating the AT tephra, Sanbe Volcano. Earth Science (Chikyu Kagaku), 56, 105–122, https://doi.org/10.15080/agcjchikyukagaku.56.2_105, 2002.

Global Volcanism Program: Volcanoes of the World (v. 5.3.4), Smithsonian Institution, compiled by Venzke [data set], https://doi.org/10.5479/si.GVP.VOTW5-2025.5.3, 2025.

Getis, A., and Ord, J. K.: The Analysis of Spatial Association by Use of Distance Statistics, Geographical Analysis, 24, 189-206, https://doi.org/10.1111/j.1538-4632.1992.tb00261.x, 1992.

Hallegatte, S., Rentschler, J., and Rozenberg, J.: Lifelines: The Resilient Infrastructure Opportunity, World Bank, https://doi.org/10.1596/978-1-4648-1430-3, 2019.

Hayes, J. L., Biass, S., Jenkins, S. F., Meredith, E. S., and Williams, G. T.: Integrating criticality concepts into road network disruption assessments for volcanic eruptions, J Appl. Volcanol., 11, 8, https://doi.org/10.1186/s13617-022-00118-x, 2022a.

https://doi.org/10.5194/egusphere-2026-5468
Preprint. Discussion started: 11 September 2026
© Author(s) 2026. CC BY 4.0 License.

Hayes, J. L., Jenkins, S. F., and Joffrain, M.: Large Uncertainties Are Pervasive in Long-Term Frequency-Magnitude Relationships for Volcanoes in Southeast Asia, Front. Earth Sci., 10, 895756, https://doi.org/10.3389/feart.2022.895756, 2022b.

He, X., and Cha, E. J.: Modeling the damage and recovery of interdependent critical infrastructure systems from natural hazards, Reliability Engineering and System Safety, 177, 162-175, https://doi.org/10.1016/j.ress.2018.04.029, 2018.

Helbing, D.: Globally networked risks and how to respond. Nature, 497, 51-59, https://doi.org/10.1038/nature12047, 2013.

Hersbach, H., Bell, B., Berrisford, P., Biavati, G., Horányi, A., Muñoz Sabater, J., Nicolas, J., Peubey, C., Radu, R., Rozum, I., Schepers, D., Simmons, A., Soci, C., Dee, D., and Thépaut, J-N.: ERA5 hourly data on single levels from 1940 to present, Copernicus Climate Change Service (C3S) Climate Data Store (CDS) [data set], DOI: 10.24381/cds.adbb2d47, 2023.

Homma, H., Miyoshi, M., and Toshida, K.: Influence of volcanic ash deposits on insulating performance of transmission insulators – Properties of volcanic ash deposition and flashover in wet condition (Report Number: H18016), Central Research Institute of Electric Power Industry, https://criepi.denken.or.jp/hokokusho/pb/reportDetail?reportNoUkCode=H18016, 2019.

Homma, H., Miyoshi, M., Takeuchi, S., and Toshida, K.: Influence of volcanic ash deposits on insulating performance of transmission insulators: Part 2 – Relation between ash fall amount and insulation deterioration (Report Number: GD23008), Central Research Institute of Electric Power Industry, https://criepi.denken.or.jp/hokokusho/pb/reportDetail?reportNoUkCode=GD23008, 2024.

International Energy Agency: Japan Electricity Security Policy, https://www.iea.org/articles/japan-electricity-security-policy, last access: March 2026, 2022.

Jenkins, S. F., Magill, C. R., and McAneney, J.: Multi-stage volcanic events: A statistical investigation, Journal of Volcanology and Geothermal Research, 161, 275–288, https://doi.org/10.1016/j.jvolgeores.2006.12.005, 2007

Jenkins, S. F., Magill, C. R., McAneney, J., and Blong, R.: Regional ash fall hazard I: a probabilistic assessment methodology.,Bull Volcanol, 74, 1699–1712, https://doi.org/10.1007/s00445-012-0627-8, 2012.

Jenkins, S. F., Wilson, T., Magill, C., Miller, V., Stewart, C., Blong, R., Marzocchi, W., Boulton, M., Bonadonna, C. and Costa, A.: Volcanic ash fall hazard and risk, in: Global Volcanic Hazards and Risk, edited by: Loughlin, S. C., Sparks, R. S. J., Brown, S. K., Jenkins, S. F., and C. Vye-Brown, Cambridge University Press, Cambridge, 173-221, https://doi.org/10.1017/CBO9781316276273.005, 2015.

Jenkins, S. F., Magill, C. R., and Blong, R. J.: Evaluating relative tephra fall hazard and risk in the Asia-Pacific region, Geosphere, 14, 492–509, https://doi.org/10.1130/GES01549.1, 2018

Jenkins, S. F., Biass, S., Williams, G. T., Hayes, J. L., Tennant, E. M., Yang, Q., Burgos, V., Meredith, E. S., Lerner, G. A., Syarifuddin, M., and Verolino, A.: Evaluating and ranking Southeast Asia's exposure to explosive volcanic hazards, Natural Hazards and Earth System Sciences, 22, 1233–1265, https://doi.org/10.5194/nhess-2021-320, 2022.

Maeno, F., Nagai, M., Nakada, S., Burden, R. E., Engwell, S., Suzuki, Y., and Kaneko, T.: Constraining tephra dispersion and deposition from three subplinian explosions in 2011 at Shinmoedake volcano, Kyushu, Japan, Bulletin of Volcanology, 76, 823, https://doi.org/10.1007/s00445-014-0823-9, 2014.

https://doi.org/10.5194/egusphere-2026-5468
Preprint. Discussion started: 11 September 2026
© Author(s) 2026. CC BY 4.0 License.

Magill, C., Wilson, T., and Okada, T.: Observations of tephra fall impacts from the 2011 Shinmoedake eruption, Japan, Earth Planets Space, 65, 677–698, https://doi.org/10.5047/eps.2013.05.010, 2013.

Maruyama, M., Yamashita, T., Hayashida, A., Hirata, T., and Danhara, T.: Examination of the relationship between the Ukinuno and Sakate Tephras from Sambe Volcano, Southwest Japan, Journal of Geography (Chigaku Zasshi), 129, 375-396, doi:10.5026/jgeography.129.375, 2020.

Matsui, S., and Inoue, T.: Pyroclastics and their Stratigraphy, Volc. Sambe. Earth Science (Chikyu Kagaku), 25, 147–163. https://doi.org/10.15080/agcjchikyukagaku.25.4_147, 1971.

Miyaji, N., Kan'no, A., Kanamaru, T., and Mannen, K.: High-resolution reconstruction of the Hoei eruption (AD 1707) of Fuji volcano, Japan, Journal of Volcanology and Geothermal Research, 207, 113–129, https://doi.org/10.1016/j.jvolgeores.2011.06.013, 2011.

Mottahedi, A., Sereshki, F., Ataei, M., Nouri Qarahasanlou, A., and Barabadi, A.: The Resilience of Critical Infrastructure Systems: A Systematic Literature Review, Energies, 14, 1571, https://doi.org/10.3390/en14061571, 2021.

Mühlhofer, E., Bresch, D. N., and Koks, E. E.: Infrastructure failure cascades quintuple risk of storm and flood-induced service disruptions across the globe, One Earth, 7, 714-729, https://doi.org/10.1016/j.oneear.2024.03.010, 2024.

Nagai, M., and Nakada, S.: Impact on the Electric Infrastructure Due to Volcanic Ash from a Hydrovolcanic Eruption of Aso Volcano in 2016, Journal of Disaster Research, 17, 829–838, https://doi.org/10.20965/jdr.2022.p0829, 2022.

Nakada, S., and Takeo, M.: 45. Asamayama, in: National Catalogue of the Active Volcanoes in Japan (The Fourth Edition, English Version), edited by: Japan Meteorological Agency and Volcanological Society of Japan, Japan Meteorological Agency, 2013.

Nakada, S., Nagai, M., Kaneko, T., Suzuki, Y., and Maeno, F.: The outline of the 2011 eruption at Shinmoe-dake (Kirishima), Japan, Earth, Planets and Space, 65, 475–488, https://doi.org/10.5047/eps.2013.03.016, 2013.

Nakano, J.: Japan's Energy Supply and Security since the March 11 Earthquake. Center for Strategic and International Studies, https://www.csis.org/analysis/japans-energy-supply-and-security-march-11-earthquake, last access: April 2026, 2011.

Newhall, C. G., and Self, S.: The volcanic explosivity index (VEI) an estimate of explosive magnitude for historical volcanism. Journal of Geophysical Research, 87, 1231, https://doi.org/10.1029/JC087iC02p01231, 1982.

Nicolas, C., Rentschler, J., Potter van Loon, A., Oguah, S., Schweikert, A., Deinert, M., Koks, E., Arderne, C., Cubas, D., Li, J., and Ichikawa, E.: Stronger Power: Improving Power Sector Resilience to Natural Hazards, World Bank, http://hdl.handle.net/10986/31910, 2019.

Nirandjan, S., Koks, E. E., Ye, M., Pant, R., van Ginkel, K. C. H., Aerts, J. C. J. H., and Ward, P. J.: Review article: Physical vulnerability database for critical infrastructure hazard risk assessments – a systematic review and data collection, Natural Hazards and Earth System Sciences, 24, 4341-4368, https://doi.org/10.5194/nhess-24-4341-2024, 2024.

Ogimoto, K., Kaizuka, I., Ueda, Y., and Oozeki, T.: A Good Fit: Japan's Solar Power Program and Prospects for the New Power System, IEEE Power and Energy Magazine, 11, 65-74, https://doi.org/10.1109/MPE.2012.2234408, 2013.

https://doi.org/10.5194/egusphere-2026-5468
Preprint. Discussion started: 11 September 2026
© Author(s) 2026. CC BY 4.0 License.

OpenStreetMap contributors: OpenStreetMap data, OpenStreetMap Foundation [data set], https://www.openstreetmap.org, downloaded: June 2025.

Organization for Cross-regional Coordination of Transmission Operators [OCCTO]: Outlook for Electricity Supply–Demand and Cross-regional Interconnection Lines: Actual Data for Fiscal Year 2024, https://www.occto.or.jp/en/information_disclosure/outlook_of_electricity_supply-demand/251110_outlook_of_electricity.html, 2025.

Ouyang, M.: Review on modeling and simulation of interdependent critical infrastructure systems, Reliability Engineering & System Safety, 121, 43-60, https://doi.org/10.1016/j.ress.2013.06.040, 2014.

Pescaroli, G., and Alexander, D.: A definition of cascading disasters and cascading effects: Going beyond the "toppling dominos" metaphor, GRF Davos Planet@Risk, 3, 58-67, https://www.preventionweb.net/quick/44129, 2015.

Rinaldi, S. M., Peerenboom, J. P., and Kelly, T. K.: Identifying, understanding, and analyzing critical infrastructure interdependencies, IEEE Control Systems Magazine, 21, 11-25, https://doi.org/10.1109/37.969131, 2001.

Schotten, R., Mühlhofer, E., Chatzistefanou, G., Bachmann, D., Chen, A. S., and Koks, E. E.: Data for critical infrastructure network modelling of natural hazard impacts: Needs and influence on model characteristics, Resilient Cities and Structures, 3, 55-65, https://doi.org/10.1016/j.rcns.2024.01.002, 2024.

Suzuki, T.: History and Future of Volcanic Disasters in and Around the Tokyo Metropolitan Area, Central Japan, in: Tokyo as a Global City: New Geographical Perspectives, edited by: Kikuchi, T., and Sugai, T., Springer, 267-285, 2018.

Thacker, S., Pant, R., and Hall, J. W.: Characterizing the Vulnerability of Future Configurations of Great Britain's Electricity Network Infrastructure to Climate-related Hazards, in: Vulnerability, Uncertainty, and Risk: Quantification, Mitigation, and Management, edited by: Beer, M., Au, S., and Hall, J. W., American Society of Civil Engineers, 648–657, https://doi.org/10.1061/9780784413609.066, 2014.

Thacker, S., Barr, S., Pant, R., Hall, J. W., and Alderson, D.: Geographic Hotspots of Critical National Infrastructure: Geographic Hotspots of Critical National Infrastructure, Risk Analysis, 37, 2490–2505, https://doi.org/10.1111/risa.12840, 2017.

Tokyo Electric Power Company Holdings [TEPCO]: Power Outage Caused by the Earthquake that occurred in Miyagi/Fukushima at 11:34 PM on March 16 [As of 3 AM, March 17], https://www.tepco.co.jp/en/hd/newsroom/press/archives/2022/20220317_01.html, last access: April 2026, 2022.

Uehara, K., and Ikeda, H.: Recent and future situation of Japan's T&D system, Journal of International Council on Electrical Engineering, 6, 231–234, https://doi.org/10.1080/22348972.2015.1129086, 2016.

Uesawa, S., Toshida, K., Takeuchi, S., and Miura, D.: Creating a digital database of tephra fallout distribution and frequency, Japan. J Appl. Volcanol., 11, 14, https://doi.org/10.1186/s13617-022-00126-x, 2022.

United Nations Office for Disaster Risk Reduction: Sendai Framework for Disaster Risk Reduction 2015-2030, UNDRR, https://www.undrr.org/quick/11409, 2015.

https://doi.org/10.5194/egusphere-2026-5468
Preprint. Discussion started: 11 September 2026
© Author(s) 2026. CC BY 4.0 License.

United Nations Office for Disaster Risk Reduction: Making Critical Infrastructure Resilient: Ensuring Continuity of Service - Policy and Regulations in Europe and Central Asia, UNDRR Regional Office for Europe, https://www.undrr.org/publication/Making%20Critical%20Infrastructure%20Resilient, 2020.

Wagner, O., Venjakob, M., and Schröder, J.: The Growing Impact of Decentralised Actors in Power Generation: A Comparative Analysis of the Energy Transition in Germany and Japan, J. sustain. dev. energy water environ. syst., 9, http://dx.doi.org/10.13044/j.sdewes.d8.0334, 2021.

Wardman, J. B., Wilson, T. M., Bodger, P. S., Cole, J. W., and Stewart, C.: Potential impacts from tephra fall to electric power systems: a review and mitigation strategies, Bull Volcanol, 74, 2221–2241, https://doi.org/10.1007/s00445-012-0664-3, 2012.

Wardman, J., Wilson, T., Hardie, S., and Bodger, P.: Influence of volcanic ash contamination on the flashover voltage of HVAC outdoor suspension insulators, IEEE Transactions on Dielectrics and Electrical Insulation, 21, 1189-1197, https://doi.org/10.1109/TDEI.2014.6832265, 2014.

Wilson, G., Wilson, T. M., Deligne, N. I., and Cole, J. W.: Volcanic hazard impacts to critical infrastructure: A review, Journal of Volcanology and Geothermal Research, 286, 148–182, https://doi.org/10.1016/j.jvolgeores.2014.08.030, 2014.

Wilson, G., Wilson, T. M., Deligne, N. I., Blake, D. M., and Cole, J. W.: Framework for developing volcanic fragility and vulnerability functions for critical infrastructure, Journal of Applied Volcanology, 6, 14, https://doi.org/10.1186/s13617-017-0065-6, 2017.

Wilson, T. M., Stewart, C., Sword-Daniels, V., Leonard, G. S., Johnston, D. M., Cole, J. W., Wardman, J., Wilson, G., and Barnard, S. T.: Volcanic ash impacts on critical infrastructure, Physics and Chemistry of the Earth, Parts A/B/C, 45–46, 5–23, https://doi.org/10.1016/j.pce.2011.06.006, 2012.

World Nuclear Association: Nuclear reactors in Japan, https://world-nuclear.org/nuclear-reactor-database/summary/Japan, last access: December 2025.

Yamamoto, T., & Nakada, S.: Chapter 14—Extreme Volcanic Risks 2: Mount Fuji, in: Volcanic Hazards, Risks, and Disasters (Vol. 1), edited by: Shroder, J. F., and Papale, P, Elsevier, 355–376, 2015.

Zhao, Y., Cai, B., Cozzani, V., & Liu, Y.: Failure dependence and cascading failure: A literature review and research opportunities, Reliability Engineering & System Safety, 256, https://doi.org/10.1016/j.ress.2024.110766, 2025.